PLOS ONE

Structure and Dynamics of the gp120 V3 Loop That Confers Noncompetitive Resistance in R5 HIV-1_{JR-FL} to Maraviroc

Yuzhe Yuan[1], Masaru Yokoyama[2], Yosuke Maeda[3], Hiromi Terasawa[3], Shinji Harada[3], Hironori Sato[2], Keisuke Yusa[4]*

1 Transfusion Transmitted Diseases Center, Institute of Blood Transfusion, Chinese Academy of Medical Science, Chenghua District, Chengdu, Sichuan Province, P. R. China, **2** Pathogen Genomics Center, National Institute of Infectious Diseases, Musashi Murayama, Tokyo, Japan, **3** Department of Medical Virology, Graduate School of Medical Sciences, Kumamoto University, Kumamoto, Japan, **4** Division of Biological Chemistry and Biologicals, National Institute of Health Sciences, Setagaya, Tokyo, Japan

Abstract

Maraviroc, an (HIV-1) entry inhibitor, binds to CCR5 and efficiently prevents R5 human immunodeficiency virus type 1 (HIV-1) from using CCR5 as a coreceptor for entry into $CD4^+$ cells. However, HIV-1 can elude maraviroc by using the drug-bound form of CCR5 as a coreceptor. This property is known as noncompetitive resistance. HIV-$1_{V3\text{-}M5}$ derived from HIV-$1_{JR\text{-}FLan}$ is a noncompetitive-resistant virus that contains five mutations (I304V/F312W/T314A/E317D/I318V) in the gp120 V3 loop alone. To obtain genetic and structural insights into maraviroc resistance in HIV-1, we performed here mutagenesis and computer-assisted structural study. A series of site-directed mutagenesis experiments demonstrated that combinations of V3 mutations are required for HIV-$1_{JR\text{-}FLan}$ to replicate in the presence of 1 μM maraviroc, and that a T199K mutation in the C2 region increases viral fitness in combination with V3 mutations. Molecular dynamic (MD) simulations of the gp120 outer domain V3 loop with or without the five mutations showed that the V3 mutations induced (i) changes in V3 configuration on the gp120 outer domain, (ii) reduction of an anti-parallel β-sheet in the V3 stem region, (iii) reduction in fluctuations of the V3 tip and stem regions, and (iv) a shift of the fluctuation site at the V3 base region. These results suggest that the HIV-1 gp120 V3 mutations that confer maraviroc resistance alter structure and dynamics of the V3 loop on the gp120 outer domain, and enable interactions between gp120 and the drug-bound form of CCR5.

Citation: Yuan Y, Yokoyama M, Maeda Y, Terasawa H, Harada S, et al. (2013) Structure and Dynamics of the gp120 V3 Loop That Confers Noncompetitive Resistance in R5 HIV-$1_{JR\text{-}FL}$ to Maraviroc. PLoS ONE 8(6): e65115. doi:10.1371/journal.pone.0065115

Editor: Jean-Pierre Vartanian, Institut Pasteur, France

Received February 14, 2013; **Accepted** April 21, 2013; **Published** June 28, 2013

Funding: This work was supported by grants from the Ministry of Health, Labour and Welfare and by the Global COE program Education and Research Center Aiming at the Control of AIDS from the Ministry of Education, Science, Sports and Culture, Japan. Y.Y. was supported by National Natural Science Foundation of China (81201329), scholarship for youth from Chinese Academy of Medical Sciences and Peking Union Medical College. The funders had no role in study design, data collection and analysis, decision to publish, or preparation of the manuscript.

Competing Interests: The authors have declared that no competing interests exist.

* E-mail: yusak@nihs.go.jp

Introduction

Inhibiting the entry of R5 human immunodeficiency virus type 1 (HIV-1) into $CCR5^+/CD4^+$ cells is an effective step in blocking viral replication. An entry inhibitor can bind to CCR5 and prevent R5 HIV-1 from using CCR5 as a coreceptor for entry [1]. Maraviroc, a CCR5 antagonist, has potent *in vitro* and *in vivo* antiviral activity against laboratory strains and clinical isolates [2–4]. Maraviroc, approved in 2007, was the first CCR5 antagonist approved by the US Food and Drug Administration and is currently used to treat patients with R5-tropic HIV-1 infections.

Treatment failures can occur because of an increasing number of pre-existing CXCR4-using viruses [5,6]. Alternatively, escape mutants can evade a CCR5 inhibitor by accumulating multiple mutations in gp120 and/or gp41 without switching their coreceptor usage [7–14]. Escape mutants can use the drug-bound form of CCR5 as a coreceptor, a property known as noncompetitive resistance [8,9,11]. In noncompetitive-resistant viruses, drug-free CCR5 usage is compatible with the additional ability of drug-bound CCR5 usage. We previously reported that a combination of polymorphic mutations in the gp120 V3 loop can confer noncompetitive resistance in HIV-$1_{JR\text{-}FL}$ [15]. One of these viruses, designated HIV-$1_{V3\text{-}M5}$, contains a set of five mutations I304V/F312W/T314A/E317D/I318V in the V3 loop (from Cys^{293} to Cys^{327}). Most other noncompetitive-resistant viruses contain multiple mutations in the V3 loop [8,9,11], although mutations reported till date in the V3 loop are not always common and resistance-associated mutations in the V3 loop were considered to be background dependent. Two elements are involved in gp120 coreceptor binding: (i) the V3 tip for the CCR5 extracellular loop 2 (ECL2) and (ii) the V3 base and stem residues and the V3 base of the gp120 core for the CCR5 N terminus [16–19]. Thus, the V3 loop of HIV-1 plays a pivotal role in its interaction with CCR5. However, how the V3 mutations induce maraviroc-resistance without changing coreceptor tropism remains unknown.

Increasing evidence indicates that the protein surface fluctuates in solution, and that such fluctuations play key roles in interactions with other molecules [20][20,23]. We previously suggested that the structural dynamics of the HIV-1 gp120 V3 loop play key roles

in modulating viral interactions with various molecules, including HIV-1 coreceptors and anti-V3 antibodies [21,22]. Therefore, it is conceivable that the V3 mutations that cause changes in the structural dynamics of the V3 loop may also be important for viral interactions with the maraviroc and CCR5 complex.

In this study, we examined how the V3 mutations, which conferred maraviroc resistance in HIV-$1_{JR\text{-}FL}$, affect the structural dynamics of the V3 loop on the gp120 outer domain. We initially performed extensive mutagenesis on the V3 loop to clarify a genetic basis for maraviroc-resistance of the HIV-$1_{JR\text{-}FL}$ strain. These studies demonstrated that combinations of V3 mutations are required to render maraviroc resistance to HIV-$1_{JR\text{-}FL}$. Subsequently, we performed MD simulations [23–25] of HIV-$1_{JR\text{-}FL}$ gp120 outer domains carrying V3 loops with and without the five maraviroc resistance mutations. The results illustrate that at the atomic-level maraviroc resistance mutations affect intrinsic structural properties and motion of the V3 loop on the HIV-1 gp120 outer domain.

Materials and Methods

Cells and Viruses

PM1/CCR5 cells were generated from the human $CD4^+$ T-cell line PM1 [26] by standard retrovirus-mediated transduction with pG1TKneo-CCR5 [27]. The cells were maintained in RPMI 1640 (Invitrogen) supplemented with 10% heat-inactivated fetal calf serum (FCS; Vitromex). MAGIC-5 cells (HeLa-$CD4^+$-$CCR5^+$-LTR-b-galactosidase) [28], used as reporter cells for HIV-1 infection, and 293T cells were maintained in Dulbecco's modified Eagle's medium (ICN Biomedicals) supplemented with 10% heat-inactivated FCS. pJR-FL was kindly provided by Prof. Koyanagi (Kyoto University).

MD simulation

HIV-1 gp120 outer domain structures with various V3 regions were constructed by the homology modeling method, using Molecular Operating Environment (MOE) software v. 2010.10 (Chemical Computing Group Inc., Montreal, Quebec, Canada) [22]. For the modeling template, we used the crystal structure of HIV-1 gp120 containing an entire V3 region at a resolution of 3.30 Å (PDB code: 2QAD) [29]. The 186 amino-terminal and 27 carboxyl-terminal residues were deleted to construct the gp120 outer domain structure. MD simulations were performed using the SANDER module of the AMBER 9 program package [30], the AMBER99SB force field [31], and the TIP3P water model [32]. Bond lengths involving hydrogen were constrained using SHAKE algorithm [32] and the time for all MD simulations was set to 2 fs. A nonbonded cutoff of 12 Å was used. After heating calculations for 20 ps until 310 K using the NVT ensemble, simulations were conducted with the NPT ensemble at 1 atm and 310 K for 20 ns. Superimposition of structures was performed by coordinating the atoms of the amino acids along the β-sheet at the gp120 core. We calculated the root mean square fluctuation (RMSF) to determine the atomic fluctuations along the trajectory broken down by residues during MD simulations. Average structures during the final 10 ns of MD simulations were used as reference structures. RMSFs were calculated using the ptraj module of AMBER 9 [22].

V3 mutant viruses

V3 mutant proviruses were constructed from pJR-FL_{an}. The 176-bp DNA fragments containing single mutations (I304V, F312W, T314A, E317D, or I318V) were subcloned into a cloning vector by overlapping PCR using primers tagged with a mutated tail. The mutation-containing DNA fragments encoding the V3 loop were repeatedly amplified from the cloning vectors using the primers VV-Af (5′-ACAGCTTAAGGAATC TGTAGAAAT-TAATTG-3′) and VV-Nh (5′-ATTTGCTAGCTATC TGTTTTAAAGTGTCAT-3′). Products were digested with AflII and NheI, subcloned into pCR-SXΔAN, and designated as pCR-SX_1, pCR-SX_2, pCR-SX_3, pCR-SX_4, and pCR-SX_5. The *Stu* I–*Xho* I fragment from the plasmids was then subcloned into pJR-FLΔSX that was created by replacing the *Stu* I–*Xho* I fragment of pJR-FL with a linker. The end products were proviral plasmids that were used for transfection for virus production. The procedure described above was repeated for construction of the proviral DNA containing two to four mutations.

For virus preparation, 293T cells (2×10^6) were transfected with 10 μg of proviral DNA using the calcium phosphate ProFection Mammalian Transfection System (Promega). The supernatant was collected 28 h after transfection, filtered through a 0.22-μm filter (Millipore), and stored at −80°C until further use. The amount of p24 Gag in the supernatant was measured by p24 Gag ELISA (Zeptometrix).

Viral replication assay

For the viral replication assay, 4×10^4 PM1/CCR5 cells were infected with 8 ng p24 Gag for 2 h in the presence or absence of 1 μM maraviroc. After washing twice with phosphate-buffered saline (PBS), the infected cells were incubated at 37°C in a 5% CO_2 atmosphere in the presence or absence of 1 μM maraviroc. On day 6 after infection, the amount of p24 Gag in the supernatant was measured by p24 Gag ELISA (Zeptometrix). Maraviroc was provided by the NIH AIDS Research and Reference Reagent Program, Division of AIDS National Institute of Allergy and Infectious Diseases.

Determination of drug susceptibility

Drug susceptibilities were determined by the single-round viral entry assay using previously titrated pseudotyped virus preparations with MAGIC-5 cells. In brief, MAGIC-5 cells were plated in 48-well tissue culture plates 1 day before infection. After absorption of the pseudotyped virus for 2 h at 37°C in the presence or absence of 1 μM maraviroc, the cells were washed twice with PBS and further incubated for 48 h in fresh medium in the presence or absence of the inhibitor.

HIV-1 single-cycle luciferase reporter assay

HIV-1 single-cycle luciferase reporter viruses were produced by cotransfection of 293T cells with pNL–LucR–E^- [33] and Env-expressing plasmids pCXN–EnvJR-FLan, pCXN–$Env_{V3\text{-}M5}$, pCXN–Env_{2345}, pCXN–Env_{1345}, pCXN–Env_{1245}, pCXN–Env_{1235}, or pCXN–Env_{1234}. Culture supernatant containing pseudoviruses at a final concentration of 1 ng/ml p24 was added to 1×10^4 cells/well MAGIC5 cells [28] in a 48-well plate. After 2 h, the cells were washed twice with phosphate-buffered saline (PBS) and firefly luciferase activity was measured 48 h postinfection, according to the manufacturer's directions (Promega).

Results

Noncompetitive-resistant virus HIV-$1_{V3\text{-}M5}$

HIV-$1_{V3\text{-}M5}$ containing the five mutations I304V/F312W/T314A/E317D/I318V in the V3 loop with a JR-FL background (Figure 1A) exhibits noncompetitive resistance to maraviroc [15]. This virus could replicate in the presence of an extremely high concentration of the entry inhibitor (Figure 1B), i.e., 1 μM maraviroc, which was 147-fold higher than the IC_{50} value of the wild-type HIV-$1_{JR\text{-}FLan}$ (0.0069 μM). HIV-$1_{V3\text{-}M5}$ could infect

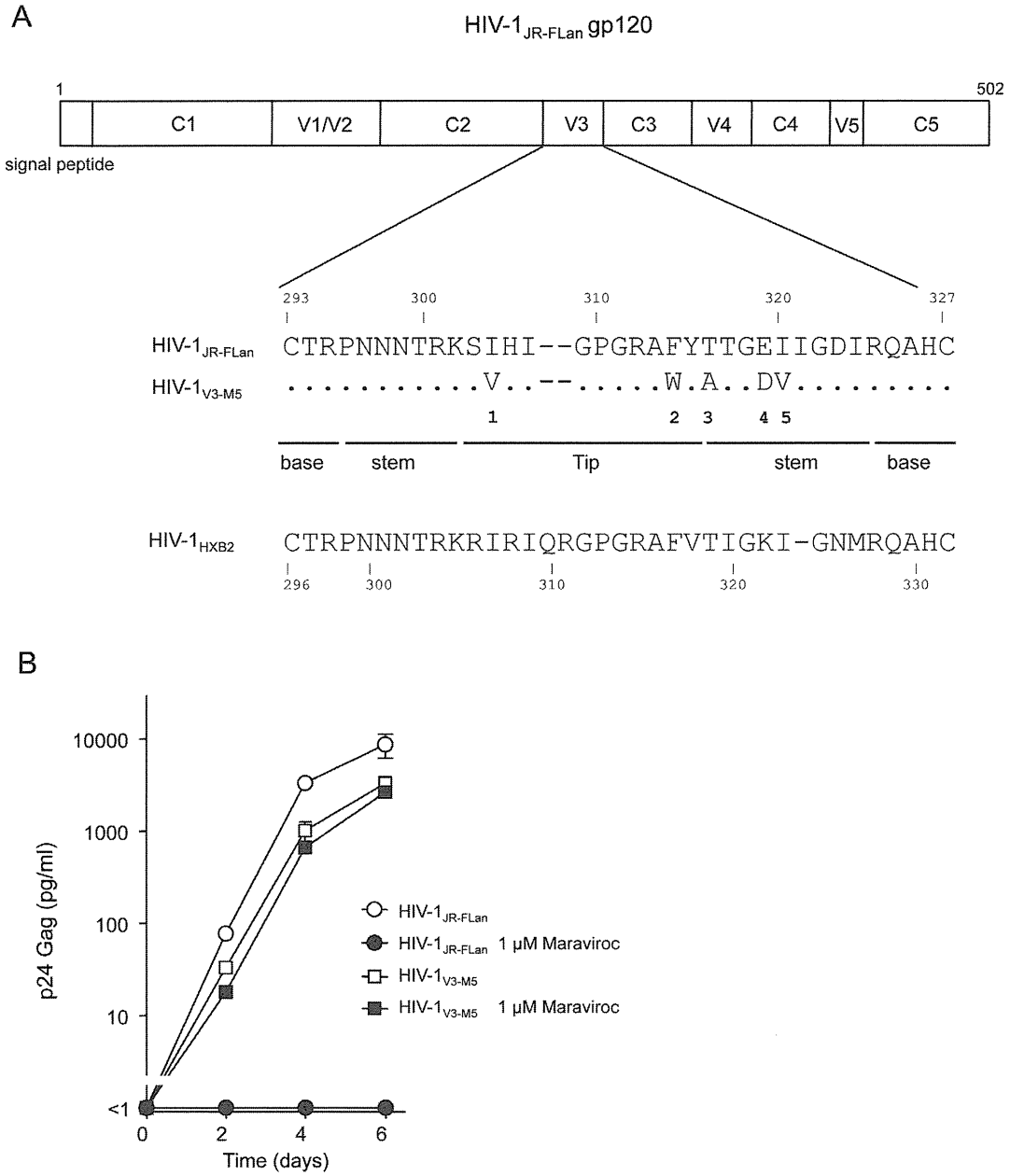

Figure 1. Noncompetitive resistant HIV-$1_{V3\text{-}M5}$. (A) Five amino acid substitutions in the V3 loop of HIV-$1_{V3\text{-}M5}$ (I304V/F312W/T314A/E317D/I318V). HIV-$1_{JR\text{-}FLan}$ was created form HIV-$1_{JR\text{-}FL}$ by incorporation of AflII and NheI. Incorporation of the NheI site led to amino acid substitutions Val^{342}-Ile^{343} to Ala^{342}-Ser^{343}. HIV-$1_{JR\text{-}FLan}$ was used as the parental virus. (B) Replication kinetics of HIV-$1_{V3\text{-}M5}$ in the presence or absence of 1 μM maraviroc in PM1/CCR5 cells. PM1/CCR5 cells (1×10^5) were infected with 10 ng of p24 Gag for 3 h. Viral replication was monitored by measuring p24 Gag in the supernatant after infection. The analysis was repeated three times; the error bars represent the S.D. of three replicates from one representative experiment.
doi:10.1371/journal.pone.0065115.g001

PM1/CCR5 cells through drug-bound CCR5 to produce p24 Gag in the presence or absence of 1 μM maraviroc, whereas HIV-$1_{JR\text{-}FLan}$ replication was completely suppressed.

Suppression of replication in recombinant viruses containing one to three mutations in the V3 loop by maraviroc

To further examine the contribution of each mutation to noncompetitive resistance, we constructed recombinant viruses containing one of the five mutations in the V3 loop (Figure 2A). I304V, F312W, T314A, E317D, and I318V were the polymorphic mutations detected in R5 clinical isolates. Thus, none of these viruses exhibited defective growth, although F312W caused a moderate decrease in p24 Gag production in the absence of maraviroc. HIV-$1_{V3\text{-}M5}$ replication was 1.8-fold lower than HIV-$1_{JR\text{-}FLan}$ replication. The presence of 1 μM maraviroc completely suppressed the production of recombinant viruses containing a single mutation, indicating that these single mutations could not confer noncompetitive resistance. Following this, we constructed 11 recombinant viruses, each containing two or three random combinations of the mutations (Figure 2B). Theoretically, the total

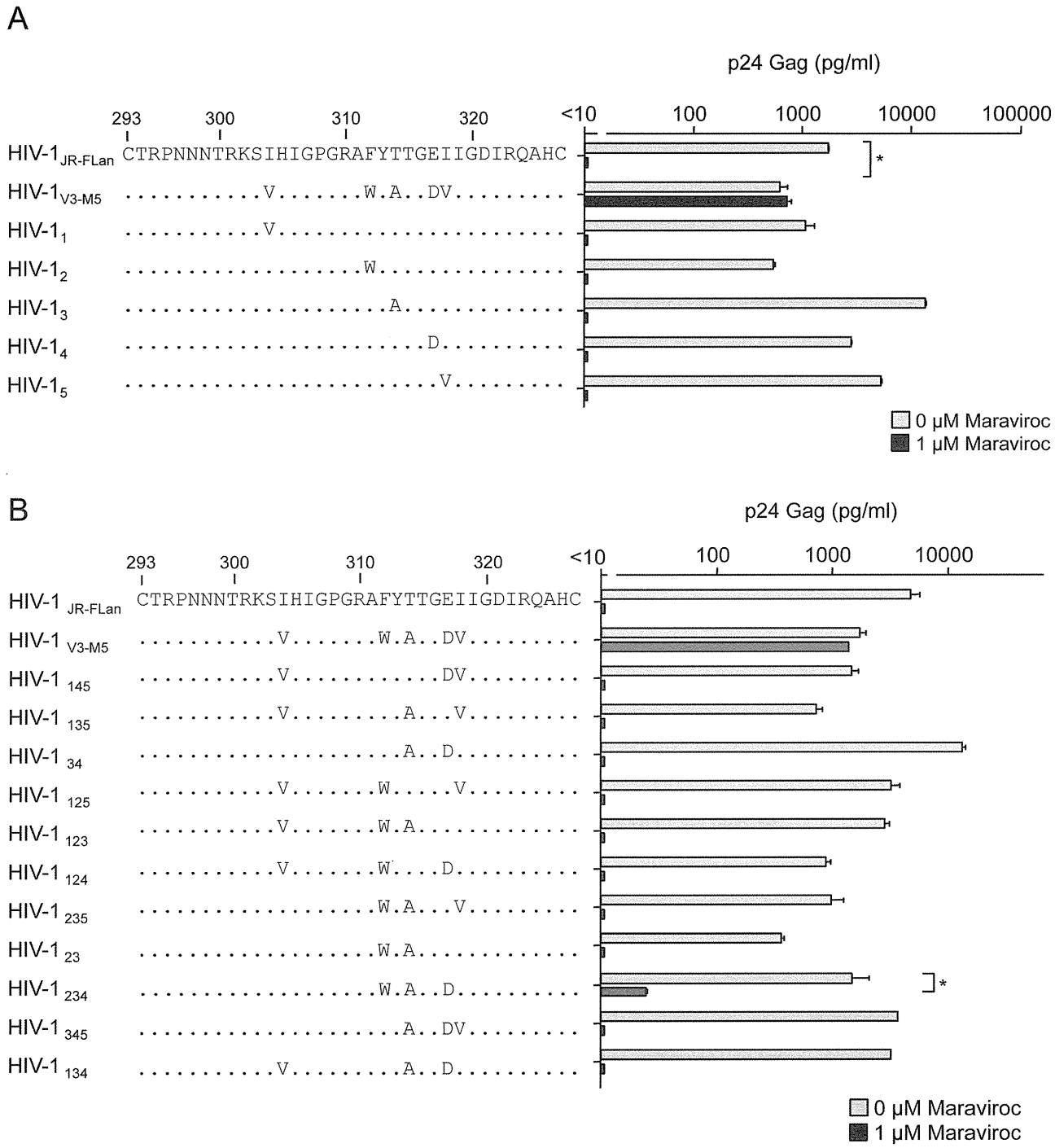

Figure 2. The effect of 1 μM of maraviroc on p24 Gag production in recombinant viruses containing one (A) and two or three (B) of the five amino acid substitutions. PM1/CCR5 cells (1×10^5) were infected with 10 ng p24 Gag for 3 h in the presence or absence of 1 μM maraviroc. On day 6 after infection, the amount of Gag in the supernatant was measured using HIV-1 p24 ELISA. The analysis was repeated three times; the error bars represent the S.D. of three replicates from one representative experiment. **, $p<0.01$. Statistical significant difference was calculated by *t* test.
doi:10.1371/journal.pone.0065115.g002

number of possible combinations of the five mutations was 120; therefore, 11 combinations of two or three mutations were insufficient to determine the crucial combination(s) for noncompetitive resistance. These recombinants could produce more than 100 pg/ml p24 Gag in the absence of maraviroc, although their replication resulted in variable levels of p24 Gag. Maraviroc mostly suppressed the replication of these recombinant viruses, indicating that the combination of these two or three mutations did not confer use of drug-bound CCR5 as a coreceptor for viral entry. However HIV-1_{234} containing F312W/T314A/E317D could replicate in the presence of 1 μM maraviroc, although p24 Gag production was 1.8% of that in its absence. We could not

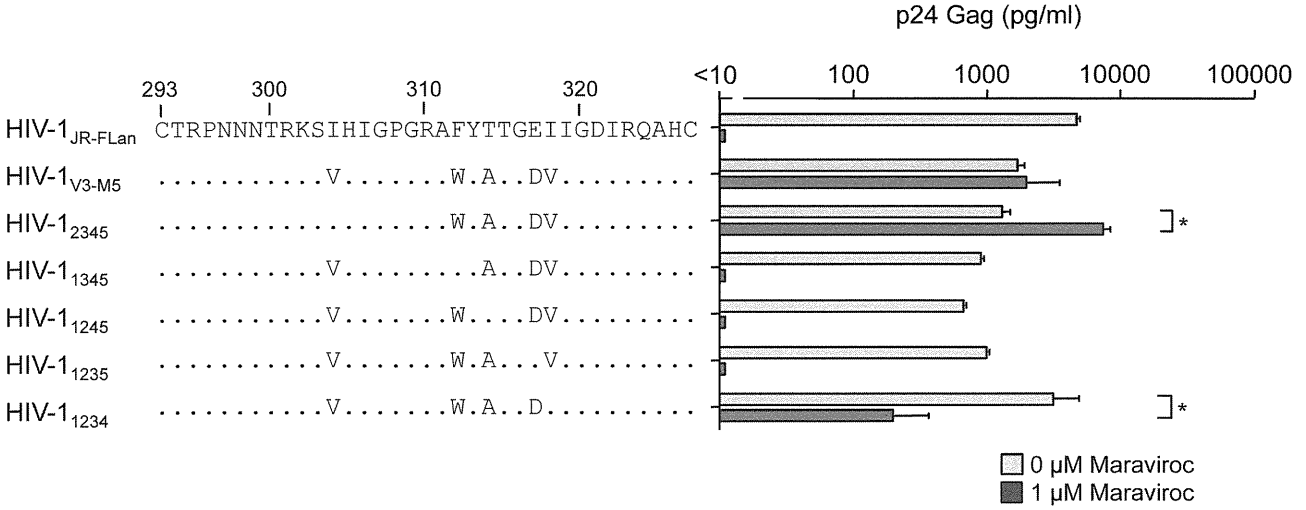

Figure 3. The effect of 1 μM of maraviroc on p24 Gag production in recombinant viruses containing four of the five amino acid substitutions. PM1/CCR5 cells (1×10^5) were infected with 10 ng p24 Gag for 3 h in the presence or absence of 1 μM maraviroc. On day 6 after infection, the amount of Gag in the supernatant was measured using HIV-1 p24 ELISA. The analysis was repeated three times; the error bars represent the S.D. of three replicates from one representative experiment. **, $p<0.01$. Statistical significant difference was calculated by *t* test.
doi:10.1371/journal.pone.0065115.g003

passage HIV-1_{234} in PM1/CCR5 cells because of its poor replication in the presence of 1 μM maraviroc (data not shown). These results suggest that HIV-1_{234} is an intermediate form in the transition of the wild type to a completely noncompetitive-resistant form.

Effect of maraviroc on recombinant viruses containing four mutations in the V3 loop

We next examined the recombinant viruses containing four mutations in the V3 loop (Figure 3). Without maraviroc, the viral fitness of HIV-1_{1234} was comparable with that of HIV-$1_{JR\text{-}FLan}$, whereas the other four recombinant viruses replicated at levels lower than those of HIV-$1_{V3\text{-}M5}$. Of note, HIV-1_{2345} and HIV-1_{1234} could replicate in the presence of 1 μM maraviroc, although HIV-1_{1345}, HIV-1_{1245}, and HIV-1_{1235} replication was completely suppressed. p24 Gag production by HIV-1_{2345} in the presence of maraviroc was 4.5-fold higher than that in its absence, whereas HIV-1_{1234} replication in the presence of maraviroc was 15-fold lower than that in the absence of maraviroc. These two viruses contained three common mutations: F312W, T314A, and E317D.

Effect of maraviroc on recombinant virus containing F312W/T314A/E317D in the V3 loop

We further examined whether HIV-1_{234} containing the triplet mutation F312W/T314A/E317D exhibited noncompetitive resistance (Figure 4). HIV-$1_{V3\text{-}M5}$ replication can be enhanced by T199K in V3 mutants to a level comparable with that in HIV-$1_{JR\text{-}FL}$ [15]. p24 Gag production by HIV-$1_{V3\text{-}M5/T199K}$ increased from 3100 pg/ml to 10,500 pg/ml in the presence of 1 μM maraviroc, whereas there was no significant increase in its absence. Similarly, HIV-$1_{234/T199K}$ replication was significantly enhanced from 31 pg/ml to 650 pg/ml in the presence of 1 μM maraviroc but not in its absence. These results indicated that triplet mutations in the V3 loop are crucial for noncompetitive resistance, and I304V, I318V, or T199K can increase viral fitness.

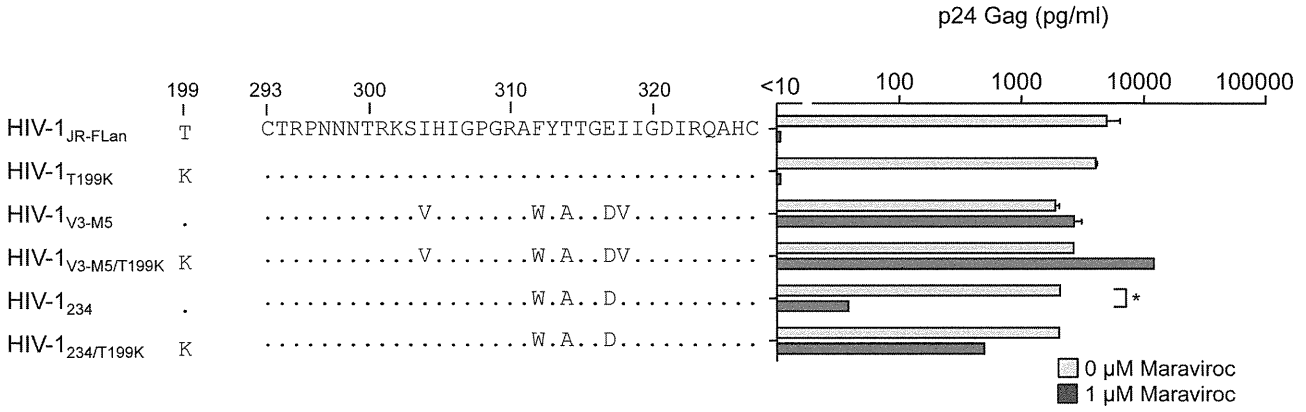

Figure 4. The effect of 1 μM of maraviroc on p24 Gag production in HIV-$1_{JR\text{-}FLan}$, HIV-1_{T199K}, HIV-$1_{V3\text{-}M5}$, HIV-$1_{V3\text{-}M5/T199K}$, HIV-1_{234}, and HIV-$1_{234/T199K}$. PM1/CCR5 cells (1×10^5) were infected with 10 ng p24 Gag for 3 h in the presence or absence of 1 μM maraviroc. On day 6 after infection, the amount of Gag in the supernatant was measured using HIV-1 p24 ELISA. The analysis was repeated three times; the error bars represent the S.D. of three replicates from one representative experiment. **, $p<0.01$. Statistical significant difference was calculated by *t* test.
doi:10.1371/journal.pone.0065115.g004

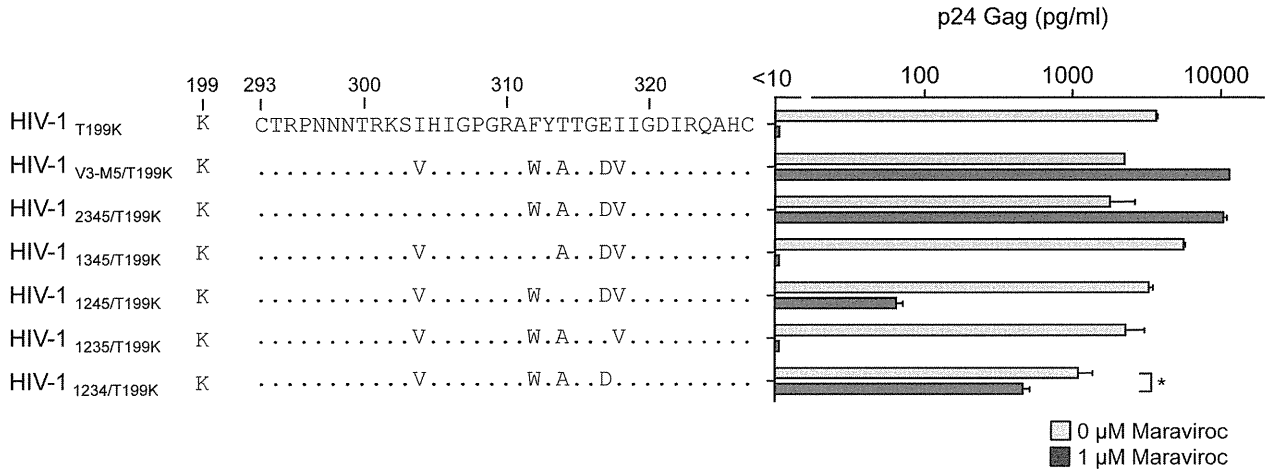

Figure 5. The effect of 1 μM of maraviroc on p24 Gag production in recombinant viruses containing four amino acid substitutions plus T199K. PM1/CCR5 cells (1×10^5) were infected with 10 ng p24 Gag for 3 h in the presence or absence of 1 μM maraviroc. On day 6 after infection, the amount of Gag in the supernatant was measured by HIV-1 p24 ELISA. The analysis was repeated three times; the error bars represent the S.D. of three replicates from one representative experiment. *, $p<0.05$; **, $p<0.01$. Statistical significant difference was calculated by *t* test.
doi:10.1371/journal.pone.0065115.g005

Finally, we examined the effects of T199K on the replication of recombinant viruses carrying four mutations in the V3 loop. In the presence of maraviroc, HIV-1_{1234} produced 6.7% of p24 Gag of that in its absence (Figure 3); however, HIV-$1_{1234/T199K}$ replication increased up to 43% (Figure 5). Of note, HIV-1_{1245} replication was completely suppressed by 1 μM maraviroc (Figure 3); however, HIV-$1_{1245/T199K}$ could replicate in the presence of 1 μM maraviroc, although the p24 production was only 2% of that in the absence maraviroc (Figure 5). These results indicated that the absence of T314A in the triplet could be compensated by I304V, I318V, or T199K and result in noncompetitive resistance.

Susceptibilities of pseudotyped viruses containing four mutations in the V3 loop to maraviroc

To confirm the phenotypes of the recombinant viruses determined by the single-round infection assay using MAGIC-5 cells, we examined the susceptibility of viral entry using pseudotyped viruses with mutant envelopes (Figure 6). The viral entry of HIV-$1_{JR\text{-}FLan}$ Env, HIV-1_{1345} Env, or HIV-1_{1235} Env was completely suppressed by maraviroc. These results were consistent with those obtained using competent viruses (Figure 3). HIV-$1_{V3\text{-}M5}$ Env inhibition with maraviroc saturated approximately 17% entry efficiency [15]. HIV-1_{1234} Env retained 4% entry efficiency in the presence of 1 μM maraviroc, indicating that the low efficiency of drug-bound CCR5 usage accounted for the low replication rate of the competent virus. In contrast, HIV-1_{2345} Env could infect MAGIC-5 cells with 41% entry efficiency of that in the absence of maraviroc (Figure 6), although viral fitness in the presence of the inhibitor was superior to that in its absence in PM1/CCR5 cells (Figure 3). Furthermore, even 1 μM maraviroc did not completely suppress HIV-1_{1245} Env entry (Figure 6). These discrepancies may have occurred because of the cell-type-specific nature of noncompetitive resistance [34].

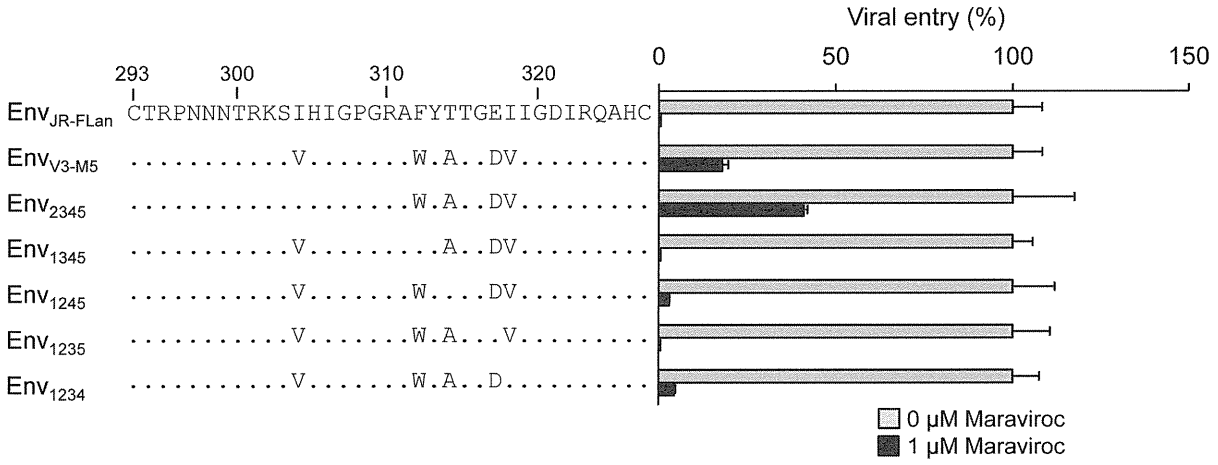

Figure 6. Maraviroc susceptibility of pseudotyped viruses derived from HIV-$1_{JR\text{-}FLan}$, HIV-$1_{V3\text{-}M5}$, HIV-1_{2345}, and HIV-1_{1345}, HIV-1_{1245}, HIV-1_{1235}, and HIV-1_{1234}. MAGIC-5 cells were infected with pseudotyped viruses in the absence or presence of 1 μM maraviroc. The analysis was repeated three times; the error bars represent the S.D. of three replicates from one representative experiment. **, $p<0.01$. Statistical significant difference was calculated by *t* test.
doi:10.1371/journal.pone.0065115.g006

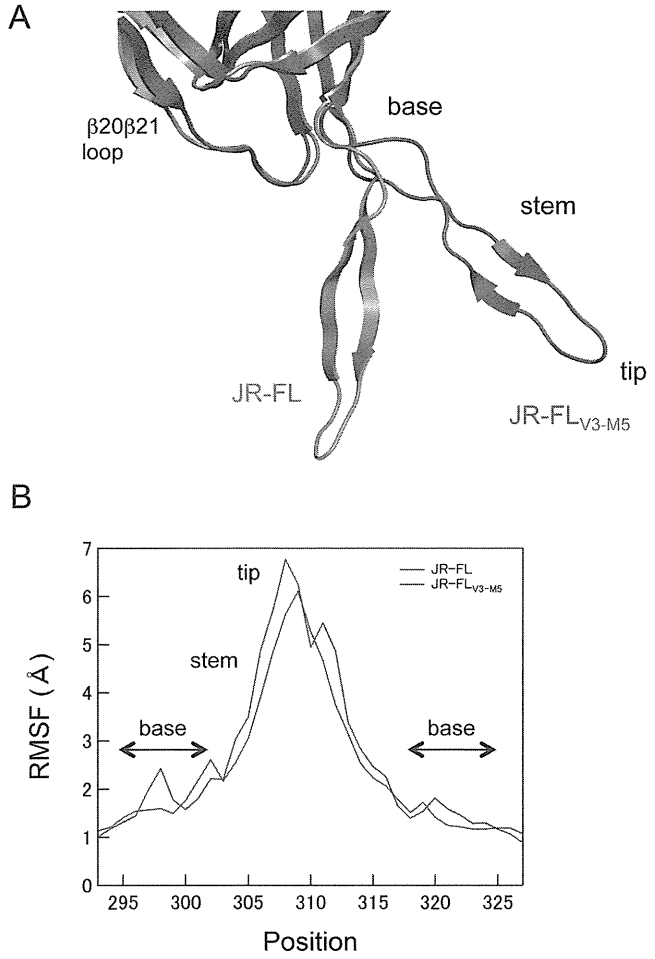

Figure 7. MD simulation of the HIV-1 gp120 outer domain. (A) Superimposition of averaged structures obtained from 40,000 snapshots during the 10–20 ns of MD simulation. Grey and blue ribbons indicate the gp120 V3 of JR-FL$_{an}$ and JR-FL$_{V3-M5}$, respectively. (B) Distribution of RMSF in the V3 region of gp120. The RMSF values indicate the atomic fluctuations of the main chains of individual amino acids during the 10–20 ns of MD simulations.
doi:10.1371/journal.pone.0065115.g007

MD simulations of the HIV-1 gp120 outer domain

MD simulation is a powerful computational method for studying motions of proteins at the atomic-scale [23–25]. To address structural impacts of the V3 maraviroc-resistance mutations, we performed MD simulations of the HIV-1$_{JR-FL}$ gp120 outer domain V3 loop with and without the five mutations of HIV-1$_{V3-M5}$ (I304V/F312W/T314A/E317D/I318V). As described previously [21,22], the root mean square deviation (RMSD) between the initial model and the model at a given time of MD simulation sharply increased soon after heating the initial model and then fluctuated continually for 20 ns of simulations (data not shown). The data suggests an intrinsic property of the gp120 outer domain V3 loops that results in structural fluctuations in solution. Hence, we constructed averaged gp120 structures using 40,000 snapshots during the 10–20 ns of MD simulation, and we superimposed them to reveal structural differences in the V3 loops of the two gp120s. Marked changes in V3 conformation were induced by introduction of the five V3 mutations (Figure 7A). The V3 loop of JR-FL$_{V3-M5}$ was located at a much more distant position from the β20β21 loop in the outer domain than that of JR-FL. In addition, an anti-parallel β-sheet in the V3 stem region was reduced in the V3 loop of JR-FL$_{V3-M5}$ compared with that of JR-FL.

To map the V3 loop sites in which fluctuations are influenced by the five mutations, we calculated the root mean square fluctuation (RMSF) of the main chains of individual amino acids in the V3 loop using 40,000 snapshots from 10–20 ns of each MD simulation (Figure 7B). The RMSF values were maximal at the V3 tip, indicating that the region involved in binding to CCR5 ECL2 fluctuates the most in solution. Interestingly, the five mutations were found to decrease the RMSF throughout the V3 tip and stem regions (Figure 7B, blue line). In addition, the five mutations caused a shift in small RMSF peaks at V3 base regions.

Discussion

In this study, we examined the genetic and structural bases for the noncompetitive resistance of HIV-1 to maraviroc. Using site-directed mutagenesis, we demonstrated that combinations of mutations in V3 are required to confer maraviroc resistance to the HIV-1$_{JR-FL}$ strain (Figures 2, 3). In addition, we showed that in combination with the V3 mutations, a T199K mutation in the C2 region enhanced viral fitness (Figures 4, 5). Finally, we indicated that these five maraviroc-resistance V3 mutations of HIV-1$_{V3-M5}$ change the intrinsic structures and motion of the V3 loop on the HIV-1 gp120 outer domain. These data provide novel insights into the molecular mechanisms of HIV-1 maraviroc resistance. Further study may be able to classify the structure of V3 loop of HIV-1 to reveal or easily develop noncompetitive resistance through antiviral treatment with maraviroc in advance.

In the V3 loop, maraviroc-associated mutations have been reported at His^{305}, Pro^{308}, Ala^{311}, Phe^{312}, Thr^{314}, Glu^{317}, and Ile^{318} (numbering in JR-FL) [11,35–37]. In the HIV-1$_{JR-FLan}$ background, F312W/T314A/E317D is a crucial combination for maraviroc resistance, and I318V was required for extensive replication comparable with that in the wild type (Figure 5). HIV-1$_{234}$ could not be passaged in PM1/CCR5 cells in the presence of 1 μM maraviroc because of its poor viral fitness (data not shown), suggesting that F312W/T314A/E317D is a type of fitness "valley" that needs to be selected on the genetic pathway for the development of noncompetitive resistance. F312W/T314A/E317D and one other mutation are required to acquire noncompetitive resistance. We could not select a maraviroc-resistant virus from the homogeneous viral population of HIV-1$_{JR-FLan}$ because spontaneous multiple mutations ($\geq$4) were unlikely to occur during *in vitro* passages, whereas our V3 virus library inherently contained F312W/T314A/E317D and fitness-enhancing mutations (I304V/I318V) [15]. We could not observe the condensation of viral clones containing one or two of these mutations at low concentrations of maraviroc (0.03–0.1 μM), suggesting that one or two combinations of these mutations did not confer a selective advantage (Figure 2). HIV-1 did not acquire maraviroc resistance by following a pathway for increasing resistance by the accumulation of multiple mutations. Instead, spontaneous alterations in the V3 loop were required to utilize maraviroc-bound CCR5. These results suggest that a virus library containing various mutations in specific regions such as the V3 loop is suitable for the *in vitro* selection of viruses resistant to entry inhibitors [38].

It remains unclear how the maraviroc resistant viruses use maraviroc-bound CCR5 as an entry coreceptor. Accumulating evidence from the investigations of protein chemistry indicates that structural fluctuations of the protein surface in solution play key roles in these molecular interactions [23–25]. Therefore, it is possible that the resistant viruses adjust these structural fluctua-

tions of coreceptor binding surfaces through V3 mutations that enable binding to maraviroc-bound CCR5. In general, it is difficult to analyze motions of proteins at an atomic scale. However, recent advances in hardware and software of biomolecular simulation have rapidly improved its precision and performance [23–25]. Therefore, in this study we applied MD simulations and elucidated the structural dynamics of the gp120 outer domain in solution.

Our MD simulations of the gp120 outer domain suggest that the five mutations in the V3 loop of HIV-$1_{V3\text{-}M5}$ caused marked changes in the physical properties of the CCR5 binding surface (Figure 7). Firstly, the mutations altered configurations and secondary structure of the tip-stem region of V3 loop on gp120. Secondly, the mutations reduced fluctuations at the base and tip regions of the V3 loop on gp120 and shifted the site of these fluctuations to the V3 base region. These results illustrate how maraviroc-resistance mutations have an impact on the intrinsic properties and structural motions of the V3 loops on the HIV-1 gp120 outer domain at the atomic-level. The altered configuration and/or fluctuation of the mutant V3 loops may advantageously support binding to drug-bound CCR5 by attenuating fluctuations on its surface. Further MD simulations in combination with experiments will clarify which of these structural changes are critical for the maraviroc resistance of HIV-1.

Author Contributions

Conceived and designed the experiments: YY KY. Performed the experiments: YY MY YM HT SH. Analyzed the data: YY MY YM SH HS KY. Contributed reagents/materials/analysis tools: YY MY YM SH HS KY. Wrote the paper: YY HS KY.

References

1. Tilton JC, Wilen CB, Didigu CA, Sinha R, Harrison JE, et al. (2010) A maraviroc-resistant HIV-1 with narrow cross-resistance to other CCR5 antagonists depends on both N-terminal and extracellular loop domains of drug-bound CCR5. J Virol 84: 10863–10876.
2. Fadel H, Temesgen Z (2007) Maraviroc. Drugs Today (Barc) 43: 749–758.
3. Tilton JC, Doms RW (2010) Entry inhibitors in the treatment of HIV-1 infection. Antiviral Res 85: 91–100.
4. Gorry PR, Ancuta P (2011) Coreceptors and HIV-1 pathogenesis. Curr HIV/AIDS Rep 8: 45–53.
5. Gulick RM, Su Z, Flexner C, Hughes MD, Skolnik PR, et al. (2007) Phase 2 study of the safety and efficacy of vicriviroc, a CCR5 inhibitor, in HIV-1-Infected, treatment-experienced patients: AIDS clinical trials group 5211. J Infect Dis 196: 304–312.
6. Moore JP, Kuritzkes DR (2009) A piece de resistance: how HIV-1 escapes small molecule CCR5 inhibitors. Curr Opin HIV AIDS 4: 118–124.
7. Westby M, van der Ryst E (2010) CCR5 antagonists: host-targeted antiviral agents for the treatment of HIV infection, 4 years on. Antivir Chem Chemother 20: 179–192.
8. Kuhmann SE, Pugach P, Kunstman KJ, Taylor J, Stanfield RL, et al. (2004) Genetic and phenotypic analyses of human immunodeficiency virus type 1 escape from a small-molecule CCR5 inhibitor. J Virol 78: 2790–2807.
9. Trkola A, Kuhmann SE, Strizki JM, Maxwell E, Ketas T, et al. (2002) HIV-1 escape from a small molecule, CCR5-specific entry inhibitor does not involve CXCR4 use. Proc Natl Acad Sci U S A 99: 395–400.
10. Marozsan AJ, Kuhmann SE, Morgan T, Herrera C, Rivera-Troche E, et al. (2005) Generation and properties of a human immunodeficiency virus type 1 isolate resistant to the small molecule CCR5 inhibitor, SCH-417690 (SCH-D). Virology 338: 182–199.
11. Westby M, Smith-Burchnell C, Mori J, Lewis M, Mosley M, et al. (2007) Reduced maximal inhibition in phenotypic susceptibility assays indicates that viral strains resistant to the CCR5 antagonist maraviroc utilize inhibitor-bound receptor for entry. J Virol 81: 2359–2371.
12. Pugach P, Marozsan AJ, Ketas TJ, Landes EL, Moore JP, et al. (2007) HIV-1 clones resistant to a small molecule CCR5 inhibitor use the inhibitor-bound form of CCR5 for entry. Virology 361: 212–228.
13. Baba M, Miyake H, Wang X, Okamoto M, Takashima K (2007) Isolation and characterization of human immunodeficiency virus type 1 resistant to the small-molecule CCR5 antagonist TAK-652. Antimicrob Agents Chemother 51: 707–715.
14. Ogert RA, Wojcik L, Buontempo C, Ba L, Buontempo P, et al. (2008) Mapping resistance to the CCR5 co-receptor antagonist vicriviroc using heterologous chimeric HIV-1 envelope genes reveals key determinants in the C2-V5 domain of gp120. Virology 373: 387–399.
15. Yuan Y, Maeda Y, Terasawa H, Monde K, Harada S, et al. (2011) A combination of polymorphic mutations in V3 loop of HIV-1 gp120 can confer noncompetitive resistance to maraviroc. Virology 413: 293–299.
16. Rizzuto CD, Wyatt R, Hernandez-Ramos N, Sun Y, Kwong PD, et al. (1998) A conserved HIV gp120 glycoprotein structure involved in chemokine receptor binding. Science 280: 1949–1953.
17. Rizzuto C, Sodroski J (2000) Fine definition of a conserved CCR5-binding region on the human immunodeficiency virus type 1 glycoprotein 120. AIDS Res Hum Retroviruses 16: 741–749.
18. Cormier EG, Dragic T (2002) The crown and stem of the V3 loop play distinct roles in human immunodeficiency virus type 1 envelope glycoprotein interactions with the CCR5 coreceptor. J Virol 76: 8953–8957.
19. Cormier EG, Tran DN, Yukhayeva L, Olson WC, Dragic T (2001) Mapping the determinants of the CCR5 amino-terminal sulfopeptide interaction with soluble human immunodeficiency virus type 1 gp120-CD4 complexes. J Virol 75: 5541–5549.
20. Thorpe IF, Brooks CL 3rd (2007) Molecular evolution of affinity and flexibility in the immune system. Proc Natl Acad Sci U S A 104: 8821–8826.
21. Yokoyama M, Naganawa S, Yoshimura K, Matsushita S, Sato H (2012) Structural dynamics of HIV-1 envelope Gp120 outer domain with V3 loop. PLoS One 7: e37530.
22. Naganawa S, Yokoyama M, Shiino T, Suzuki T, Ishigatsubo Y, et al. (2008) Net positive charge of HIV-1 CRF01_AE V3 sequence regulates viral sensitivity to humoral immunity. PLoS One 3: e3206.
23. Ode H, Nakashima M, Kitamura S, Sugiura W, Sato H (2012) Molecular dynamics simulation in virus research. Front Microbiol 3: 258.
24. Karplus M, Kuriyan J (2005) Molecular dynamics and protein function. Proc Natl Acad Sci U S A 102: 6679–6685.
25. Dodson GG, Lane DP, Verma CS (2008) Molecular simulations of protein dynamics: new windows on mechanisms in biology. EMBO Rep 9: 144–150.
26. Lusso P, Earl PL, Sironi F, Santoro F, Ripamonti C, et al. (2005) Cryptic nature of a conserved, CD4-inducible V3 loop neutralization epitope in the native envelope glycoprotein oligomer of CCR5-restricted, but not CXCR4-using, primary human immunodeficiency virus type 1 strains. J Virol 79: 6957–6968.
27. Maeda Y, Foda M, Matsushita S, Harada S (2000) Involvement of both the V2 and V3 regions of the CCR5-tropic human immunodeficiency virus type 1 envelope in reduced sensitivity to macrophage inflammatory protein 1alpha. J Virol 74: 1787–1793.
28. Hachiya A, Aizawa-Matsuoka S, Tanaka M, Takahashi Y, Ida S, et al. (2001) Rapid and simple phenotypic assay for drug susceptibility of human immunodeficiency virus type 1 using CCR5-expressing HeLa/CD4(+) cell clone 1–10 (MAGIC-5). Antimicrob Agents Chemother 45: 495–501.
29. Huang CC, Tang M, Zhang MY, Majeed S, Montabana E, et al. (2005) Structure of a V3-containing HIV-1 gp120 core. Science 310: 1025–1028.
30. Case DA, TAD, Cheatham III TE, Simmerling CL, Wang JM, et al. (2006) AMBER 9. San Francisco: University of California.
31. Hornak V, Abel R, Okur A, Strockbine B, Roitberg A, et al. (2006) Comparison of multiple Amber force fields and development of improved protein backbone parameters. Proteins 65: 712–725.
32. Jorgensen WL, Chandrasekhar J, Madura JD, Impey RW, Klein ML (1983) Comparison of simple potential functions for simulating liquid water. J Chem Phys 79: 926–935.
33. Mariani R, Rutter G, Harris ME, Hope TJ, Krausslich HG, et al. (2000) A block to human immunodeficiency virus type 1 assembly in murine cells. J Virol 74: 3859–3870.
34. Roche M, Jakobsen MR, Sterjovski J, Ellett A, Posta F, et al. (2011) HIV-1 escape from the CCR5 antagonist maraviroc associated with an altered and less-efficient mechanism of gp120-CCR5 engagement that attenuates macrophage tropism. J Virol 85: 4330–4342.
35. Tilton JC, Amrine-Madsen H, Miamidian JL, Kitrinos KM, Pfaff J, et al. (2010) HIV type 1 from a patient with baseline resistance to CCR5 antagonists uses drug-bound receptor for entry. AIDS Res Hum Retroviruses 26: 13–24.
36. Maeda Y, Yoshimura K, Miyamoto F, Kodama E, Harada S, et al. (2011) In vitro and In vivo Resistance to Human Immunodeficiency Virus Type 1 Entry Inhibitors. AIDS Clin Res.
37. Berro R, Klasse PJ, Jakobsen MR, Gorry PR, Moore JP, et al. (2012) V3 determinants of HIV-1 escape from the CCR5 inhibitors Maraviroc and Vicriviroc. Virology 427: 158–165.
38. Yusa K, Maeda Y, Fujioka A, Monde K, Harada S (2005) Isolation of TAK-779-resistant HIV-1 from an R5 HIV-1 GP120 V3 loop library. J Biol Chem 280: 30083–30090.

Citation: Molecular Therapy—Nucleic Acids (2013) 2, e137; doi:10.1038/mtna.2013.64

www.nature.com/mtna

Promoter Targeting shRNA Suppresses HIV-1 Infection *In vivo* Through Transcriptional Gene Silencing

Kazuo Suzuki[1], Shinichiro Hattori[2], Katherine Marks[1], Chantelle Ahlenstiel[3], Yosuke Maeda[4], Takaomi Ishida[5], Michelle Millington[6], Maureen Boyd[6], Geoff Symonds[1,6], David A Cooper[1,3], Seiji Okada[2] and Anthony D Kelleher[1,3]

Despite prolonged and intensive application, combined antiretroviral therapy cannot eradicate human immunodeficiency virus (HIV)-1 because it is harbored as a latent infection, surviving for long periods of time. Alternative approaches are required to overcome the limitations of current therapy. We have been developing a short interfering RNA (siRNA) gene silencing approach. Certain siRNAs targeting promoter regions of genes induce transcriptional gene silencing. We previously reported substantial transcriptional gene silencing of HIV-1 replication by an siRNA targeting the HIV-1 promoter *in vitro*. In this study, we show that this siRNA, expressed as a short hairpin RNA (shRNA) (shPromA-JRFL) delivered by lentiviral transduction of human peripheral blood mononuclear cells (PBMCs), which are then used to reconstitute NOJ mice, is able to inhibit HIV-1 replication *in vivo*, whereas a three-base mismatched variant (shPromA-M2) does not. In shPromA-JRFL–treated mice, HIV-1 RNA in serum is significantly reduced, and the ratio of $CD4^+/CD8^+$ T cells is significantly elevated. Expression levels of the antisense RNA strand inversely correlates with HIV-1 RNA in serum. The silenced HIV-1 can be reactivated by T-cell activation in *ex vivo* cultures. HIV-1 suppression is not due to offtarget effects of shPromA-JRFL. These data provide "proof-of principle" that an shRNA targeting the HIV-1 promoter is able to suppress HIV-1 replication *in vivo*.

Molecular Therapy—Nucleic Acids (2013) **2**, e137; doi:10.1038/mtna.2013.64; published online 3 December 2013
Subject Category: siRNAs, shRNAs, and miRNAs Therapeutic proof-of-concept

Introduction

Currently available combined antiretroviral therapy has markedly improved both morbidity and mortality associated with human immunodeficincy cirus (HIV)-1 infection, reducing the viral load ((VL) HIV-1 RNA in serum) and rescuing $CD4^+$ T cells from HIV-1 infection.[1–4] However, HIV-1 persists in its proviral form in cellular reservoirs.[5–7] On cessation of even prolonged combined antiretroviral therapy, rapid viral recrudescence occurs in the overwhelming majority of cases.[8,9] Alternative therapeutic approaches are required to overcome these limitations. We have been investigating a transcriptional gene silencing (TGS) approach using short interfering RNAs (siRNAs) gene targeting the promoter region of HIV-1. Unlike siRNA targeting HIV-1 messenger RNA (mRNA), which induces the post-TGS (PTGS) pathway to degrade mRNA in the cytoplasm, we and others have shown that specific siRNAs targeting viral promoter regions can induce TGS within the nucleus.[10–16] TGS has also been demonstrated in an *in vivo* model targeting the promoter of vascular endothelial growth factor (VEGF-A).[17]

Although initial reports demonstrated inhibition of HIV-1 replication by siRNA through PTGS,[18,19] further *in vitro* studies revealed a number of modes of resistance: directly, through rapid development of mutations within[20–22] or near the siRNA targeted region,[23] and indirectly, via mutations in regions separate from the RNA interference targets.[24] Nonetheless, both direct and indirect modes of resistance compromise the efficacy of combinations of siRNAs targeting multiple HIV mRNA regions.[25] Therefore, PTGS approaches appear to have fundamental limitations.

siRNA-induced TGS was originally reported in plants.[26–29] TGS has more recently been observed in certain mammalian cells.[11,30,31] TGS has potential advantages over PTGS when silencing of HIV is the objective. The high mutation rate of HIV-1, due to its nonproof reading reverse transcriptase (RT) and high replication rates, allows rapid adaptation to environmental pressures including the development of resistance or escape mutations.[32,33] As TGS results in marked reduction of HIV-1 transcription through induction of epigenetic modifications in the HIV-1 promoter,[34] production of new viral RNA is limited and the HIV-1 RT enzyme has no substrate on which to act. Therefore, resistance mutations are less likely to develop in a TGS approach.[16] However, TGS approaches may have their own pitfalls. Offtarget effects must be carefully excluded as they have been described with siRNAs or antisense RNA designed to induce TGS.[35] Sequence-specific offtarget effects are difficult to predict and even slight offsetting of target sequences can make substantial changes to the extent of offtarget effects.[36] Furthermore, sequence-nonspecific offtarget effects can be induced by the triggering of interferon (IFN) pathways by double-stranded RNA through endosomal receptors such as Toll-like receptor (TLR)3, TLR7, and TLR8.[37,38]

We have reported sustained, profound, highly specific viral suppression of viral replication by siRNA- and short heparin RNA (shRNA)–induced TGS of HIV-1 and simian immunodeficiency virus in various *in vitro* models, through a mechanism that results in chromatin compaction.[34,39–42] Because HIV-1 has identical long terminal repeats (LTRs) at the 5′ and 3′ ends of the integrated virus, any promoter-targeted siRNA

[1]St. Vincent's Centre for Applied Medical Research, Darlinghurst, New South Wales, Australia; [2]Center for AIDS Research, Kumamoto University, Kumamoto, Japan; [3]The Kirby Institute, The University of New South Wales, New South Wales, Australia; [4]Department of Medical Virology, Faculty of Life Sciences, Kumamoto University, Kumamoto, Japan; [5]Research Center for Asian Infectious Disease, Institute of Medical Science, University of Tokyo, Tokyo, Japan; [6]Calimmune, Sydney, Australia. Correspondence: Kazuo Suzuki, St. Vincent's Centre for Applied Medical Research Darlinghurst, New South Wales, Australia. E-mail: k.suzuki@amr.org.au
Received 21 August 2013; accepted 23 September 2013; advance online publication 3 December 2013. doi:10.1038/mtna.2013.64

can potentially act through PTGS. With our lead candidate, called PromA, we have found that the contribution of PTGS is limited.[34] In this study, we used a lentiviral delivery system to express the previously described shRNA targeting the HIV-1 promoter region to transduce human PBMCs. We first assessed shRNA-mediated TGS approach using a PBMC infection model *in vitro*. We then demonstrated an antiviral effect of this construct on HIV-1 infection *in vivo* using NOJ mice[43] transplanted with the lenivirus-transduced PBMCs.

Results

shRNA targeting the promoter of HIV-1_{JRFL} suppresses viral expression in PBMCs obtained from healthy donors

Our previous *in vitro* TGS studies were based on PromA targeting the NF-κβ region of the U3 promoter region of HIV-1 (**Figure 1a**). The humanized NOD/SCID Janus kinase 3 knockout mice model has been developed to use the HIV-1_{JRFL} strain.[43] We sequenced the HIV-1_{JRFL} promoter region, which demonstrated that there was a one-base mismatch compared with the original sequence targeted by PromA (**Figure 1a**). Because induction of TGS is sequence specific, and a two-base mismatched siRNA failed to induce effective TGS *in vitro*,[42] we constructed U6 promoter driven–shRNA expression self-inactivated lentivirus vector plasmids with a GFP expression unit (**Figure 1b**) specifically targeting this region of HIV_{JRFL} (shPromA-JRFL), as well as shPromA-M2, a three-base mismatched control, and shPromA-Sc (a scrambled control) (**Figure 1b**). VSV-G envelope pseudotype lentiviruses expressing each of these constructs were used to transduce human PBMCs. A transduction efficiency of 38.4% for shPromA-JRFL, 31.7% for shPromA-M2, and 34.7% for shPromA-Sc was achieved as assessed by EGFP expression 5 days after transduction (**Figure 1c**). PBMCs transduced with shPromA-JRFL, but not those transduced with control lentivirus, challenged with HIV-1 *in vitro*, showed significant reduction of HIV-1 *gag* mRNA (**Figure 1d**).

The detection of *gag* mRNA reflects transcription of unspliced viral RNA. We also investigated whether the transcription of spliced viral RNA was modulated by shPromA-JRFL by measuring levels of spliced-*tat* RNA (**Figure 1e**). As expected, shPromA-JRFL spliced-*tat* expression was significantly reduced, but with a different kinetic to the suppression of *gag* RNA. This results in a marked difference in the kinetics of the ratio of spliced (*tat*): unspliced (*gag*) RNA in the shPromA-JRFL–treated cultures compared with the control cultures with a peak in the spliced:unspliced ratio at day 7 (**Figure 1f**). By day 14, the levels of both *gag* and spliced-*tat* RNA are similar in each of the cultures, consistent with loss of effect. Sequence of the virus obtained from the culture supernatant of PBMCs transduced with lenti-shPromA-JRFL at day 14 did not show any mutations in U3 region and, in particular, in the shRNA target sequence. Given that only 38.4% of cells in these bulk cultures were transduced, these results suggest that the elevated HIV-1 replication by day 14, as assessed by both spliced and unspliced viral RNA, is likely due to overgrowth of virus from untransduced cells. Having demonstrated the *in vitro* efficacy of our new construct, we proceeded to *in vivo* experiments using shPromA-M2 as a control, because this three-base mismatched control is a more rigorous specificity control than the scrambled shPromA sequence.

shPromA-JRFL inhibits HIV-1 replication in a humanized NOJ mouse model

We evaluated the *in vivo* antiviral effect of shPromA-JRFL in a previously established model of acute HIV-1 infection based on the nonobese diabetic (NOD)/SCID/Janus kinase 3 knockout (NOJ) mice reconstituted with human PBMCs and then infected with HIV_{JRFL}.[43] First, we transduced healthy human PBMCs with lentivirus-expressing shPromA-JRFL or shPromA-M2. Transduction efficiency before transplantation was 22% for shPromA-JRFL and 25% for shPromA-M2. Seven days later, mice (n = 8 per group) were transplanted with 1×10^7 (nonselected) lentivirus-transduced PBMCs per-mouse by intraperitoneal injection and the cells allowed to engraft. Five days later, mice were infected by intraperitoneal inoculation of HIV-1_{JRFL} (**Figure 2a**). This is a model of rapidly progressive HIV-1 infection with high VLs, massive $CD4^+$ T-cell depletion, and profound immunodeficiency occurring within weeks of infection.[43]

Mononuclear cells were recovered at sacrifice (day 14 after HIV-1 infection) from the peritoneal cavity and the spleen. VL in serum was detected by RT quantitative real-time PCR (RT-qPCR). VL in the mice transplanted with PBMCs expressing shPromA-JRFL was significantly lower (P = 0.014) than in shPromA-M2 control mice (**Figure 2b**). $CD4^+$ T cells were reduced relative to $CD8^+$ T cells in shPromA-M2–transplanted mice, whereas the $CD4^+$ to $CD8^+$ T-cell ratio was better preserved in mice transplanted with shPromA-JRFL both in the peritoneal cavity (P = 0.038) and in the spleen (P = 0.002) (**Figure 2c**). Furthermore, the extent of downregulation of CD4 surface expression is reduced by shPromA-JRFL (**Supplementary Figure S1**). Thus, shPromA-JRFL appears to protect $CD4^+$ T cells against HIV-1–mediated depletion and downregulation of CD4 surface expression. By contrast, there was no significant difference in $CD8^+$ T-cell numbers between the two groups, indicating successful human PBMC engraftment in all the mice (**Supplementary Figure S2**). Intracellular staining after gating on human $CD3^+$ $CD8^-$ spleen cells demonstrated that the percentage of p24-expressing ($p24^+$) cells was significantly lower in the mice transplanted with shPromA-JRFL–transduced PBMCs (P = 0.014) (**Figure 2d**).

Expression levels of the antisense strand of shPromA-JRFL inversely correlated with VL

The above data indicate a reduction in viral replication and relative protection from $CD4^+$ T-cell destruction, but there was substantial variability in the extent of these effects among the mice within the PromA-JRFL–treated group. Previous observations have suggested that the antisense strand of double-stranded siRNA is responsible for induction of TGS in mammalian cells.[14,39,44] After transduction of the shPromA-JRFL lentivirus, the shRNA expression unit is transcribed from the U6 promoter, by RNA polymerase III, which terminates at a poly(T) motif within this expression unit. The short hairpin loop sequence is then processed by cellular ribonucleases to form mature/processed double-stranded siRNA.[45] We, therefore, quantified the antisense strand of the shPromA-JRFL transcript by real-time PCR, as previously described,[42] to

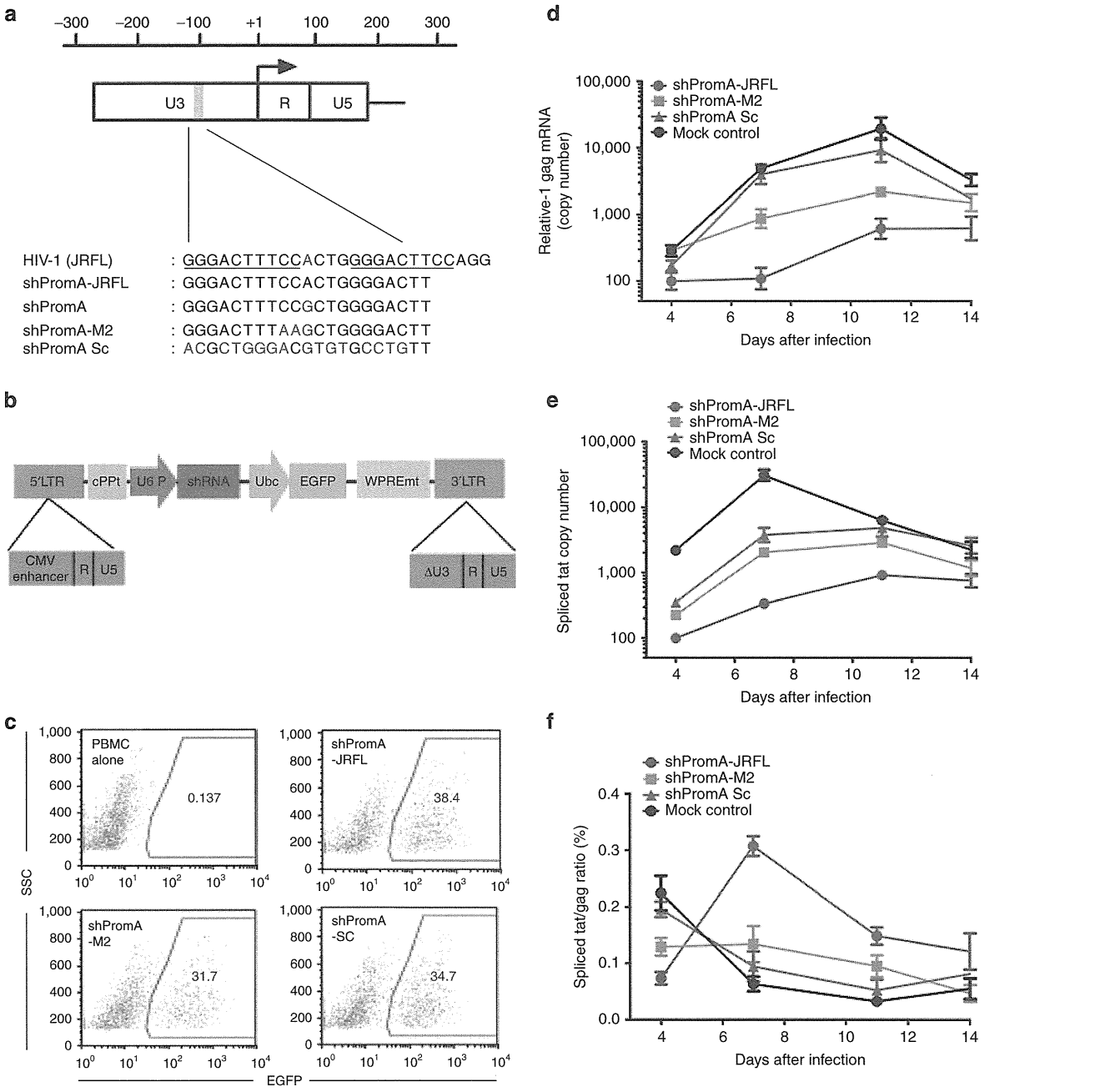

Figure 1 Human immunodeficiency virus (HIV)-1 transcription is inhibited by lenti-shPromA-JRFL in peripheral blood mononuclear cells (PBMCs). (**a**) Alignment of self-inactivating (SIN) lentivirus vector constructs along with HIV-1_{JRFL} target sequences. A map of HIV-1 5′ long terminal repeat (LTR) region is illustrated: the blue bar indicates the location of NF-κβ binding region; the arrow indicates the HIV-1 transcription start site; red text in the alignment highlights nucleic acids that differ from the HIV-1_{JRFL} sequence; numbers indicate the nucleic acid location relative to the transcription start site; and underlined text indicates NF-κβ binding region in the HIV-1 promoter. (**b**) Structure of SIN lentivirus vector. SIN vector consists of central polypurine tract (cPPT), U6 promoter (U6 P), short hairpin RNA (shRNA), ubiquitin C promoter (Ubc), and enhanced green fluorescent protein (EGFP). WPREmt, mutant woodchuck promoter response element, and modified LTR, allow integration but not expression of viral genome. We constructed U6 promoter–driven shRNA expression SIN lentivirus vector plasmid with EGFP expression unit targeting shPromA-JRFL, shPromA-M2 (three-base mismatched control), and shPromA-Sc (scramble control). (**c**) Expression of EGFP after transduction of lenti-shPromA, shM2, shSc into PBMCs. PBMCs prepared from a healthy donor were stimulated with interleukin-2 for 6 hours, followed by transduction of the lentivirus with a multiplicity of infection of 10. Five days later, EGFP expression was determined by flow cytometric analysis. (**d**) HIV-1 transcription is inhibited in PBMCs transduced by lenti-shPromA-JRFL. 2×10^6 transduced PBMCs were infected with 50 ng HIV-1_{JRFL}, as determined by the reverse transcriptase assay. The cell-associated HIV *gag* messenger RNA (mRNA) copy number normalized to 1,000 copies of GAPDH is shown along with time after HIV-1_{JRFL} infection. (**e**) HIV-1 spliced-*tat* expression is modulated in PBMCs transduced with lenti-shPromA-JRFL. Spliced-*tat* mRNA copy number normalized to 1,000,000 copies of GAPDH is shown following after HIV-1_{JRFL} infection. (**f**) The ratio of spliced-*tat* over unspliced HIV-1 mRNA, measured by HIV-1 *gag* mRNA, is shown following HIV-1_{JRFL} infection. In panels **d**, **e**, and **f** the mean values and SEM of three independent experiments are plotted.

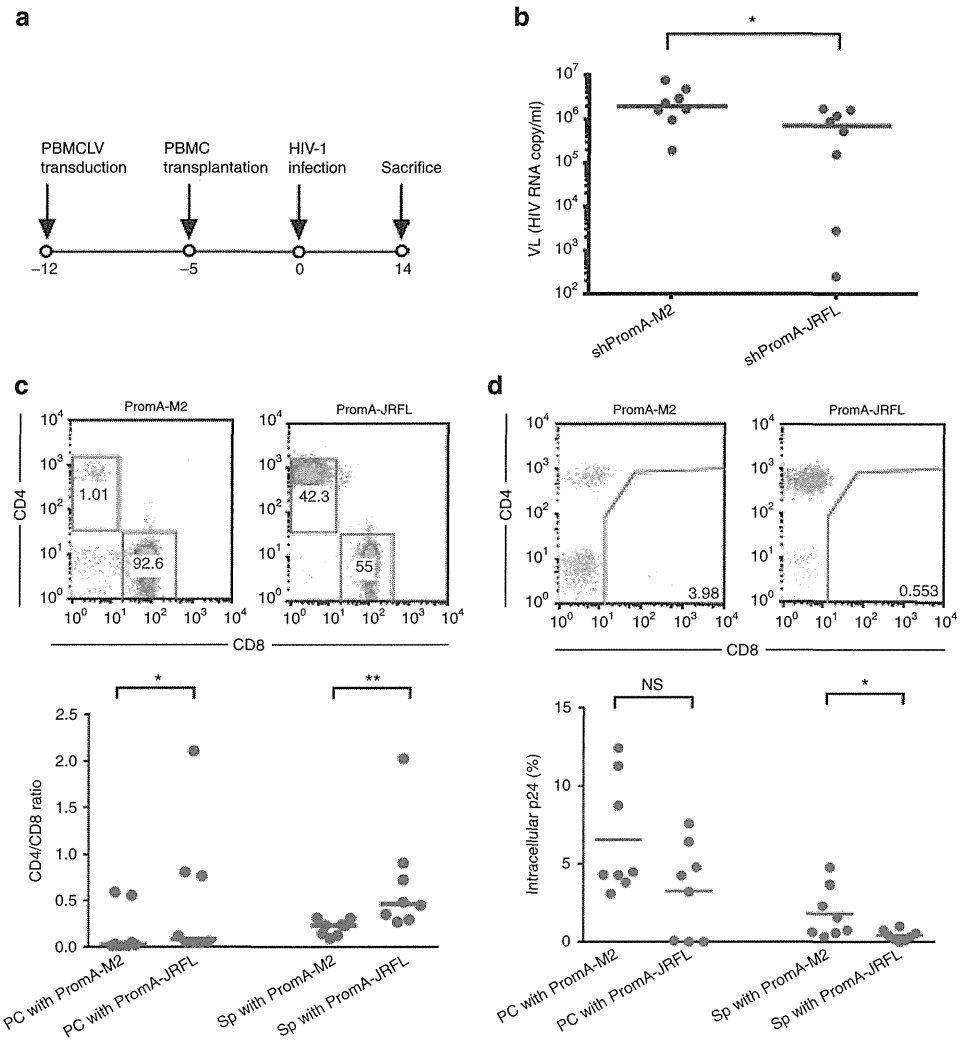

Figure 2 Transduction with lentivirus-shPromA-JRFL shows antiviral effects in NOJ mouse. (**a**) Time line for *in vivo* NOJ mouse experiment. LV denotes lentivirus. (**b**) Amount of viral load (VL) (HIV-1 RNA in serum) in mice with lentivirus-transduced peripheral blood mononuclear cells (PBMCs). Blood samples were collected from mice orbit on day 14 after HIV-1_{JRFL} infection. Horizontal bars indicate the medians. $^{*}P < 0.05$. (**c**) Effects on the ratio of $CD4^{+}/CD8^{+}$ cells in mice with lentivirus-transduced PBMCs. Short bars indicate the medians. $^{*}P < 0.05$, $^{**}P < 0.01$. (**d**) Effect on intracellular p24-positive cells. Peritoneal cavity cells and splenocytes recovered on day 14 after HIV-1 inoculation were analyzed by flow cytometry. The percentage of p24-positive cells among $CD4^{+}$ T cells (gated as $mCD45^{-}$ $hCD45^{+}$ $hCD3^{+}$ $hCD8^{-}$) is shown ($n = 8$). Horizontal bars indicate the medians. $^{*}P < 0.05$. NS, not significant; PC, peritoneal cavity; Sp, Spleen.

determine whether the degree of expression and processing of the shRNA constructs impacted the antiviral effects. It was found that the degree of antisense-strand expression had a strong inverse correlation with VL in serum in the mice transplanted with PromA-JRFL–transduced PBMCs ($r = 0.83$; $P = 0.0015$), but not in those transplanted with the control shRNA PromA-M2 ( ). Similarly, there was an inverse correlation between expression of cell-associated HIV-1 *gag* mRNA in $CD4^{+}$ T cells from the spleen and expression antisense strand of the shPromA-JRFL ($r = 0.84$; $P = 0.0014$; **Supplementary Figure S3a**) and strong linear correlation between VL and expression of cellular-associated HIV-1 *gag* mRNA in CD4 cells ($r = 0.84$; $P = 0.0014$; **Supplementary Figure S3b**). Consistent with these observations, there was a strong linear correlation between VL and both the percentage of p24-positive $CD3^{+}$ $CD8^{-}$ cells ($r = 0.98$; $P < 0.0001$; **Figure 3b**) and the cell-associated viral mRNA from splenocytes ($r = 0.84$; $P = 0.0014$) in shPromA-JRFL–expressing mice, indicating that serum VL correlates with cellular expression of HIV-1 Gag protein in $CD4^{+}$ T cells and *gag* mRNA in splenocytes. These data all point to the fact that the presence of the processed antisense strand of shPromA-JRFL is a strong correlate of inhibition of viral replication.

Phorbol myristate acetate, a strong stimulating reagent, reactivates silenced transcription of HIV-1 in *ex vivo* culture

Latent HIV-1 has silenced transcription, which is able to be switched on by strong cellular activating stimuli such as phorbol myristate acetate (PMA).[46] The U1 cell line is a latently infected monocytoid cell line that contains the proviral form of HIV-1, with heterochromatin formation in the viral promoter

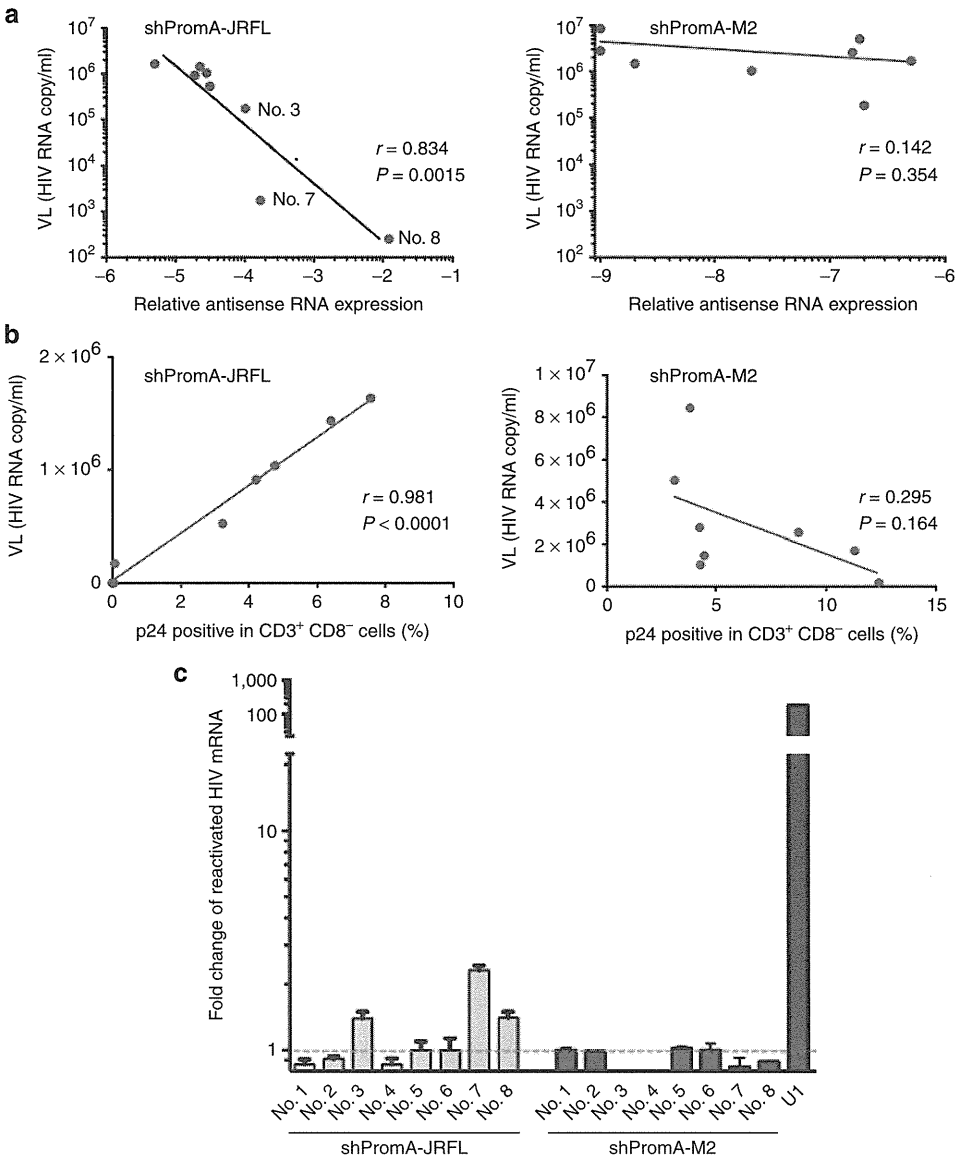

Figure 3 Transcriptional gene silencing (TGS) is induced by lenti-shPromA-JRFL. (**a**) Inverse correlation of expression level of the antisense strand of shPromA-JRFL and viral load (VL). Relative antisense RNA expression of shPromA-JRFL was detected by the primer-specific reverse transcriptase–polymerase chain reaction. (**b**) Linear correlation of intracellular p24 expression level and VL. Intercellular p24 staining in $CD3^+$ $CD8^-$ cells obtained from peritoneal cavity was analyzed by flow cytometry and was plotted against VL. (**c**) Transcriptionally suppressed human immunodeficiency virus (HIV)-1 is reactivated by phorbol myristate acetate (PMA). Splenocytes recovered from day 14 after inoculation of $HIV\text{-}1_{JRFL}$ were divided into two cultures with or without addition of PMA. After *ex vivo* culture for 24 hours, cellular-associated messenger RNA (mRNA) was extracted for analysis of HIV *gag* mRNA. Substantially increased expression of HIV-1 *gag* mRNA was found after PMA activation in three mice with highly suppressed HIV-1 (Nos. 3, 7, and 8), obtained from shPromA-JRFL treated mice. U1 is a positive control for HIV-1 latently infected cells. The mean values and SEM of three independent experiments are plotted.

region, the 5′LTR. The silenced provirus can be activated by treatment of cells with PMA with concomitant relaxation and opening of the chromatin structure.[47–49] Given that we have previously shown that si/shPromA acts by inducing biochemical changes in histone tails resulting in a heterochromatic structure associated with the 5′LTR, we hypothesized that the silenced HIV-1 induced by shPromA-JRFL would be activated by PMA. We conducted *ex vivo* culture of the splenic $CD4^+$ T cells from all mice in the shPromA-JRFL–treated group, including the three highly suppressed mice (nos. 3, 7, and 8, as indicated in **Figure 3a**). We found that PMA treatment resulted in elevated levels of *gag* mRNA in the PBMCs from the three suppressed mice, but not in those where VL was poorly suppressed. Of note, these were the same mice in which the antisense strand of shPromA-JRFL was poorly expressed (**Figure 3c**). We also found that PMA treatment did not increase the levels of *gag* mRNA in the PBMCs from the 8 mice treated with shPromA-M2 (**Figure 3c**). These data are consistent with TGS induced by shPromA-JRFL being responsible for the observed suppression of HIV-1 transcription.

We also confirmed the activation of HIV-1 transcription using an *in vitro* experimental model. We transduced PM1-CCR5 T cells, with lenti-shPromA-JRFL. We conducted limiting dilution of transduced PM1-CCR5 T cells to isolate strongly positive EGFP clonal populations (**Figure 4a,b**). After confirming expression of EGFP in more than 99% of cells in this clone, (PromA-JRFL No.3), we infected these cells with two concentrations of HIV-1_{JRFL} (**Figure 4c**). We also measured the expression level of the antisense strand of the shPromA-JRFL transcript by RT-qPCR in PM1-ccr5 cells in the presence of ongoing active HIV-1_{JRFL} infection. HIV infection did not make a difference to the expression levels of the antisense strand of the shPromA-JRFL transcript (**Supplementary Figure S4a,b**).[42] After confirming that shPromA-JRFL–expressing PM1-CCR5 cells completely suppressed HIV-1 replication, we then assessed whether activation of the suppressed HIV-1 transcription could be induced by various stimuli, including PMA and the histone deacetylase inhibitor, tricostatin A (**Figure 4d**). Both stimuli resulted in reactivation of viral replication, with tricostatin A having a greater effect than that of PMA. The powerful effect of tricostatin A in viral reactivation in the presence of shPromA-JRFL strongly suggests that this shRNA is causing viral suppression through TGS, because recruitment of histone deacetylase is a classic mark of TGS. It is interesting that not all activation stimuli result in reactivation of Prom-A–suppressed infection. GM-CSF stimulation of untransduced U1 cells results in reactivation of latent virus. However, GM-CSF stimulation of U1 cells lentivirally transduced to express shPromA did not result in increased viral replication (**Supplementary Figure S5**). These data are concordant with our previous *in vitro* data, demonstrating that siRNA and shPromA cause suppression of HIV-1 replication through TGS.[34,40,41] The data also suggest that TGS mediated through shRNA can be sustained even in the presence of certain cytokines, such as GM-CSF.

TGS induced by shPromA-JRFL was not associated with offtarget effects

Endosomal innate immune receptors, such as TLR3, TLR7, and TLR8, recognize long single- or double-stranded RNAs, triggering type I IFN and IFN-stimulated gene expression that can result in viral suppression by both nonspecific offtarget effects and undesirable toxicities.[37,38] We evaluated the extent of induction of IFN-α gene expression using RT-qPCR on splenocytes from shPromA-JRFL, shPromA-M2, and untreated mice. We used polyI:C (polyinosinepolycytosine)-treated PBMCs as a positive control.[50,51] There was no difference in IFN-α expression levels (**Figure 5a**). Furthermore, by RT-qPCR there was no difference in expression of the IFN-α response genes, OSA1, ISG20, and IFIT1 between groups of mice (**Figure 5b**), which is consistent with a lack of induction of IFN.

To exclude offtarget effects mediated through the targeting by shPromA-JRFL of other NF-κβ binding motifs of host genes as distinct from the NF-κβ motif in the HIV-1 LTR, a PCR-based assay was used to assess the expression levels of 86 NF-κβ-driven host genes, including IFN-α, β, and γ. The shPromA-JRFL was not associated with altered expression of NF-κβ driven host genes, including the IFN genes (**Supplementary Figure S6a,b**). These data are concordant

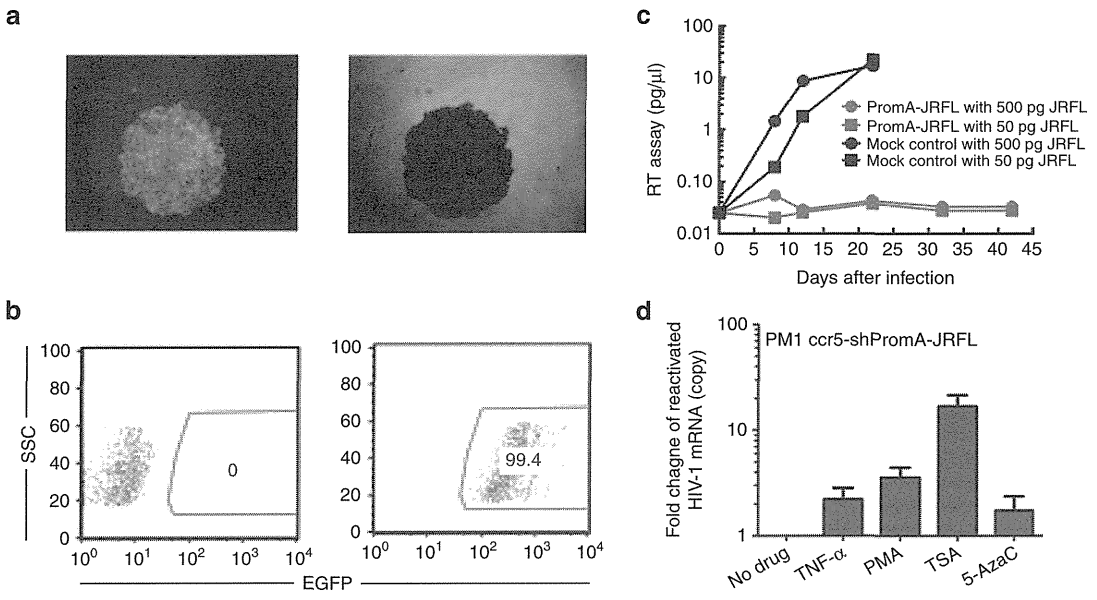

Figure 4 Transcriptional gene silencing (TGS) is induced by lenti-shPromA-JRFL *in vitro*. (**a**) PM1-ccr5 cells were transduced with lenti-shPromA with a multiplicity of infection of 10, subjected to limited dilution to isolate EGFP-positive colonies. A fluorescent image of clone PromA-JRFL No. 3. is shown on the left and the corresponding phase contrast image is on the right. (**b**) Expression of EGFP after expansion of clone PromA-JRFL No.3 as determined by flow cytometric analysis. (**c**) HIV-1 replication is inhibited in Lenti-shPromA-JRFL–transduced PM1-ccr5 cells. HIV-1 in the culture supernatant was detected by the colorimetric reverse transcriptase (RT) assay. (**d**) HIV-1 transcription is reactivated from the transcriptionally suppressed PM1-ccr5 cells, transduced with Lenti-shPromA-JRFL. 24 hours after activation with PMA or TSA, cell-associated mRNA was extracted for analysis of HIV *gag* mRNA. Fold change of reactivated HIV-1 *gag* mRNA is shown. 5Aza, 5-azacytidine; PMA, phorbol myristate acetate; TNF-α, tumor necrosis factor-α; TSA, trichostatin A. The mean values and SEM of three independent experiments are plotted.

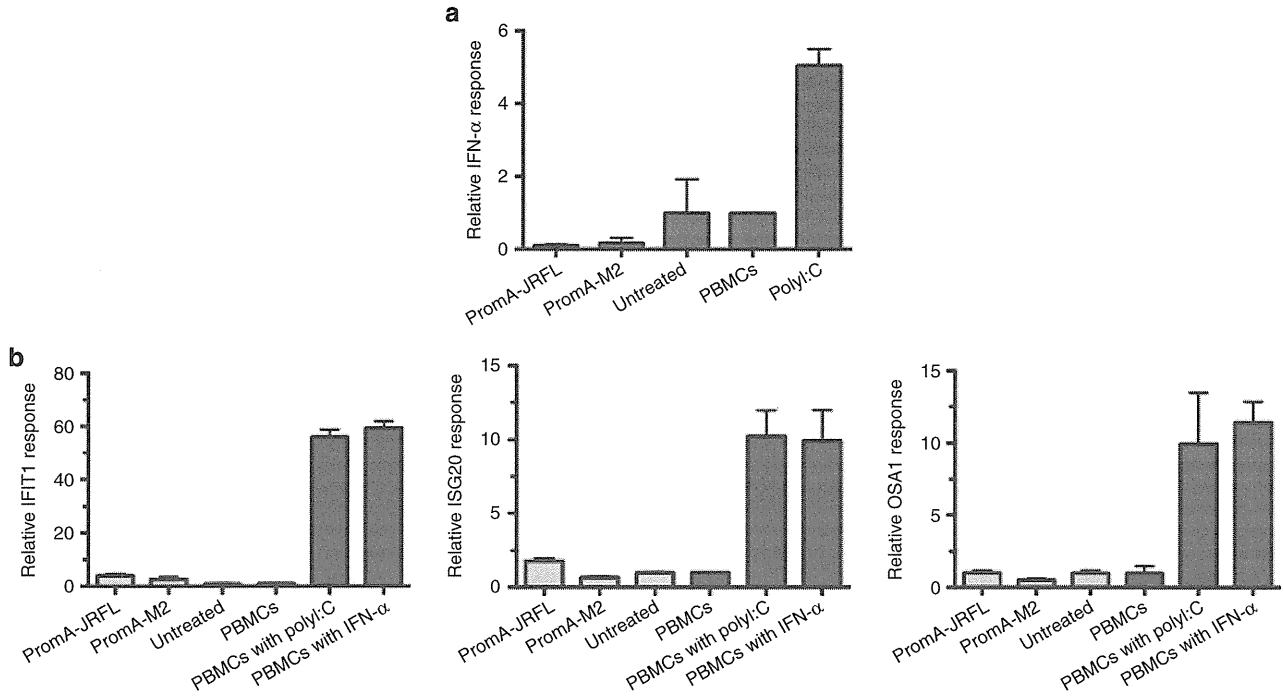

Figure 5 No significant offtarget effects are induced by lenti-shPromA-JRFL. (**a**) Effect of lentiviral transduction of peripheral blood mononuclear cells (PBMCs) on interferon-α (IFN-α) expression. Splenocytes were prepared from mice transplanted with lentivirus-transduced PBMCs. Cell-associated messenger RNA (mRNA) was extracted for analysis of IFN-α by reverse transcriptase–polymerase chain reaction (RT-PCR). PolyI:C–treated PBMCs were used a positive control, indicated in dark blue. (**b**) Effect of lentiviral transduction of PBMCs on IFN response genes. Cell-associated mRNA was extracted for analysis of three IFN-α response genes (OSA1, ISG20, and IFITM1) by RT-PCR. PolyI:C or IFN-α–treated PBMCs were used as positive controls, these are indicated in dark blue. The mean values and SEM of three independent experiments are plotted.

to our previous analyses of offtarget effects induced by siRNA and shRNA forms of PromA in HeLa and MOLT-4 cell and strongly suggest that the observed HIV-1 suppression is not the result of offtarget effects induced by shPromA-JRFL.[42]

Discussion

Our previous *in vitro* data based on HeLa or T-cell lines suggested that TGS of HIV-1 can be induced by promoter targeted si/shRNAs through the induction of epigenetic modifications to form heterochromatin structures, which resemble the biochemical modifications of the HIV-1 promoter in latently infected cell lines.[12,13] In this report, we extend our si/shRNA-mediated TGS approach into an *in vivo* NOJ humanized mouse model.[43] Although there are several reports of PTGS mediated by siRNA using *in vivo* humanized mouse models,[50–54] this report demonstrates that HIV-1 gene silencing based on the TGS pathway is possible *in vivo*. Our NOJ model is a model of acute rapidly progressive HIV infection in which massive infection occurs: hCD4/CD8 cell ratio significantly decreases, and high VL is achieved within 14 days of intraperitoneal inoculation of $HIV\text{-}1_{JRFL}$.[43] Despite this highly activated, destructive, and rapidly progressive infection with high levels of viral transcription, we were still able to successfully demonstrate a degree of viral suppression using an shRNA that induces transcriptional silencing.

We demonstrated substantial antiviral effects that resulted in significant alterations in a number of surrogate markers of disease progression in the shPromA-JRFL–treated group, including reduced serum VL, reduced percentage of HIV Gag p24 protein–positive $CD3^+$ $CD8^-$ T cells, and an improved ratio of $CD4^+/CD8^+$ T cells. Of note, the extent of each of these effects correlated with the extent of expression of the processed shRNA antisense strand. These data also suggest that in mice that showed adequate expression of the antisense strand of shPromA-JRFL in $CD4^+$ T cells, there was an observable HIV-1 antiviral effect, which we conclude is occurring through TGS. Because the $CD4^+$ T cells were relatively protected from active HIV-1 infection through shPromA-JRFL–mediated TGS, we could see significant reduction of VL in serum in shPromA-JRFL mice. The data from the *in vitro* PBMC experiments show that shPromA-JRFL has marked effects on production of both spliced and unspliced viral mRNA. Reduction in the production of spliced-*tat* is likely to be important in the effective silencing of latently infected cells, as Tat, through its interaction with the TAR region of the 5′LTR allows efficient upregulation of transcription of long unspliced HIV-1 mRNA.[55–57] Furthermore, the *ex vivo* reactivation of HIV-1 infection by PMA stimulation is consistent with our previously reported observations that siPromA and shPromA constructs result in viral suppression by TGS[40,41] and with other models of HIV-1 latency.[47–49,58] In addition, the *ex vivo* reversal of viral suppression by TNF-α and, in particular, by the histone deacetylase inhibitor, tricostatin A, is consistent with suppression being induced by TGS. We confirmed that shPromA-JRFL did not induce any significant offtarget effects, determined by expression of type

I and II IFNs, IFN response genes and NF-κβ–regulated host genes. We also demonstrated that not all activating stimuli reverse this process, for example, the GM-CSF–induced activation of latent HIV-1 in shPromA–transduced U1 cell was inhibited.

This acute human PBMC-NOJ mouse model has been used to demonstrate proof of principle of potential *in vivo* efficacy of shPromA delivered by a retroviral vector, focusing on the relative protection of human CD4+ T cells against HIV-1 infection. To further this approach, we are investigating the use of newborn NOJ mouse engrafted via intrahepatic injection of human cord blood–derived CD34+ cells transduced with retroviral constructs expressing shPromA and appropriate controls.[59] This will enable us to evaluate the effect of this approach on engraftment and hematopoietic cell differentiation and reconstitution, and subsequently on HIV-1 infection. An advantage of the CD34+ NOJ model is that the cell number required in this model is 100-fold lower (5×10^4 CD34+ cells per mouse) than that of required in the current NOJ mouse model reconstituted by human PBMCs (1×10^7 PBMCs per mouse). The titer of our current lentiviruses is ~2×10^8 infectious viral particle per milliliter. Therefore, a higher multiplicity of infection can be achieved to obtain a greater transduction rate, which will potentially provide greater efficacy.

Using the CD34+ cell–reconstituted NOJ model, we wish to explore a scenario closer to that which we envisage these constructs will be used in human HIV-1 treatment, primarily on cessation of antiretroviral drugs in controlled chronic infection to determine whether lentivirally delivered shPromA constructs can stabilize the viral reservoir on withdrawal of antiretroviral therapy. If the latent viral reservoir could be maintained as effectively silenced by shPromA treatment, these constructs would represent a substantial step forward on the road toward a functional cure, by providing an alternative to the currently proposed eradication strategies than using various viral transcription activating agents, such as histone deacetylase and demethylases.[49,60,61] Rather than activating virus and abolishing infected cells, we propose that constructs such as shPromA could be used to lock HIV-1 into latency maintaining transcriptionally inactive virus even in patients ceasing conventional antiretroviral therapy, thus achieving a prolonged remission or functional cure of HIV-1 infection.

Materials and methods

Production of lentivirus. The construction of lentiviral vector lenti-shPromA-JRFL, lenti-shPromA-M2, and lenti-Sc were previously described.[41] An outline of the construction of self-inactivated lentivirus vector plasmid with GFP expression unit is illustrated in **Figure 1b**. Vesicular stomatitis virus-G (VSV-G) pseudotyped lentiviral vectors were prepared by transduction of plasmid DNA into 293T cells using HilyMax (Dojindo Molecular Technologies, Osaka, Japan), a lipofectamine-based transfection reagent. The resulting virus was concentrated from supernatant as previously described[62,63], and stocks were titrated on 293T cells based on EGFP expression.

PBMC transduction with lentivirus. Peripheral blood was collected from healthy volunteers after informed consent was obtained, according to the institutional guidelines approved by the Faculty of Life Sciences and Pharmaceutical Sciences, Kumamoto University, Kumamoto, Japan. Healthy donor PBMCs were prepared by standard density gradient centrifugation using Ficoll-Hypaque (VWR, Murarrie, Australia). Cells were cultured in RPMI-1640 medium supplemented with penicillin (100 U/ml), streptomycin (100 μg/ml), 20% fetal calf serum (R20) in the presence of 20 units/ml of interleukin-2 (Roche Diagnostic, Castle, Hill, Australia) for 7 hours, followed by overnight transduction with either lenti-shPromA-JRFL, lenti-shPromA-Sc, or lenti-shPromA-M2 using a multiplicity of infection of 1.5–2.0. Cells were then cultured in R20 for a further 7 days before transplantation.

Transplantation of human PBMCs into NOJ mice and HIV-1 infection of mice. Human PBMC-transplanted NOJ (hu-PBMC-NOJ) mice were generated as described previously.[43] Briefly, NOJ mice were irradiated (1.0 Gy), and bulk lenti-shPromA-JRFL– or lenti-shPromA-M2–transduced PBMCs (1×10^7) were resuspended in phosphate-buffered saline (PBS) (0.1 ml) and infused intraperitoneally into each mouse. Seven days after PBMC implantation, a dose of 200 ng of HIV-1_{JRFL}, which was determined by HIV-1 p24 antigen ELISA (ZeproMetrix), suspended in 0.1 ml of PBS, was inoculated intraperitoneally into each mouse. On day 14 after HIV-1_{JRFL} infection, mice were killed and blood samples were collected from the mouse orbit, and peritoneal cavity and spleen cells were harvested and resuspended in PBS (see **Figure 2a**). All animal experiments were performed according to the guidelines of the Kumamoto University Graduate School of Medical Science.

RT-PCR analysis and RT assay. Cellular RNA was extracted using High Pure RNA Tissue Kit (Roche Diagnostic), followed by the RT-PCR analysis as described previously.[39,42] Detection of spliced-*tat* was conducted using the same RT-PCR conditions with the primer set: Tat-F: ATG GAG CCA GTA GAT CCT AGA CTA and Tat-B: ATT CCT TCG GGC CTG TCG using RT-PCR (SensiFAST Probe one-step RT-PCR: Bioline). Both HIV-1 *gag* mRNA and spliced-*tat* mRNA levels were normalized against GAPDH. Colorimetric RT activity (RT assay) in culture supernatants was determined as previously described.[64]

Flow analysis of CD4+ CD8+ T cells and internal p24 staining. Lymphocyte subsets from human mononuclear cells obtained from the transplanted mice were characterized by flow cytometric analysis as described previously.[43] Briefly, cells were treated with red cell lysing buffer (155 mM NH_4Cl, 10 mM $KHCO_3$, and 0.1 mM EDTA) to lyse erythrocytes, and single-cell suspensions were prepared in staining medium (PBS with 2% fetal bovine serum and 0.05% sodium azide) and stained with monoclonal antibodies: allophycocyanin (APC)-Cy7–conjugated antimouse CD45 (BD Pharmingen, Kobe, Japan), APC-conjugated anti-hCD4 (Dako, Tokyo, Japan), phycoerythrin-Cy7–conjugated anti-hCD3 (e-Bioscience, Tokyo, Japan), Pacific Blue–conjugated anti-hCD8 (BioLegend, Tokyo, Japan), and Pacific Orange–conjugated antihuman CD45 (anti-hCD45) (Invitrogen, Tokyo, Japan). After 30 minutes, cells were washed twice and fixed in PBS with 1% paraformaldehyde for 20 minutes and permeabilized in PBS with 0.1% saponin. After a 10-minute incubation, cells were

stained with phycoerythrin-conjugated anti-HIV-1 p24 monoclonal antibody (Beckman Coulter, Tokyo, Japan) for 30 minutes. All washes and staining procedures were conducted at 4 °C. Following staining, the cells were analyzed on an LSR II flow cytometer (BD Bioscience). Data were analyzed with FlowJo software (Tree Star, Tokyo, Japan).

Statistical analysis. RT-PCR analysis and RT assay values are given as mean and SEM. Ratio of $CD4^+/CD8^+$ cells and VL were tested for significance using a nonparametric Mann–Whitney *U* test. A *P* value <0.05 was considered statistically significant. All analyses were performed using GraphPad Prism Version 5.0a (Graphpad Software, San Diego, CA).

Supplementary material

Figure S1. Effects of lenti-shPromA-JRFL and lenti-shPromA-M2 on $CD4^-$ T cells.
Figure S2. Effects of lenti-shPromA-JRFL and lenti-shPromA-M2 on $CD8^+$ T cells.
Figure S3. HIV-1 gag HIV mRNA level is inhibited through TGS induced by lenti-shPromA-JRFL.
Figure S4. The antisense strand expression level is not altered with HIV-1JRFL infection.
Figure S5. Activation of latent HIV-1–infected U1 cells is inhibited by lenti-shPromA.
Figure S6. No significant difference in comparison of 86 NF-κβ driven genes in PBMCs trasduced with lenti-shPromA.

Acknowledgments. The authors thank the Australian Government Department of Health and Ageing (RM07292) and National Health and Medical Research Council (455350 to A.K. and 630571 for K.S. and C.H.). Funding for open-access charge was provide by St. Vincent's Centre for Applied Medical Research.

1. Ho, DD, Neumann, AU, Perelson, AS, Chen, W, Leonard, JM and Markowitz, M (1995). Rapid turnover of plasma virions and CD4 lymphocytes in HIV-1 infection. *Nature* **373**: 123–126.
2. Mellors, JW, Rinaldo, CR Jr, Gupta, P, White, RM, Todd, JA and Kingsley, LA (1996). Prognosis in HIV-1 infection predicted by the quantity of virus in plasma. *Science* **272**: 1167–1170.
3. Perelson, AS, Essunger, P, Cao, Y, Vesanen, M, Hurley, A, Saksela, K *et al.* (1997). Decay characteristics of HIV-1-infected compartments during combination therapy. *Nature* **387**: 188–191.
4. Palella, FJ Jr, Delaney, KM, Moorman, AC, Loveless, MO, Fuhrer, J, Satten, GA *et al.* (1998). Declining morbidity and mortality among patients with advanced human immunodeficiency virus infection. HIV Outpatient Study Investigators. *N Engl J Med* **338**: 853–860.
5. Chun, TW, Finzi, D, Margolick, J, Chadwick, K, Schwartz, D and Siliciano, RF (1995). *In vivo* fate of HIV-1-infected T cells: quantitative analysis of the transition to stable latency. *Nat Med* **1**: 1284–1290.
6. Finzi, D, Hermankova, M, Pierson, T, Carruth, LM, Buck, C, Chaisson, RE *et al.* (1997). Identification of a reservoir for HIV-1 in patients on highly active antiretroviral therapy. *Science* **278**: 1295–1300.
7. Siliciano, RF and Greene, WC (2011). HIV latency. *Cold Spring Harb Perspect Med* **1**: a007096.
8. Wong, JK, Hezareh, M, Günthard, HF, Havlir, DV, Ignacio, CC, Spina, CA *et al.* (1997). Recovery of replication-competent HIV despite prolonged suppression of plasma viremia. *Science* **278**: 1291–1295.
9. Chun, TW, Justement, JS, Moir, S, Hallahan, CW, Maenza, J, Mullins, JI *et al.* (2007). Decay of the HIV reservoir in patients receiving antiretroviral therapy for extended periods: implications for eradication of virus. *J Infect Dis* **195**: 1762–1764.
10. Turner, AM, De La Cruz, J and Morris, KV (2009). Mobilization-competent Lentiviral Vector-mediated Sustained Transcriptional Modulation of HIV-1 Expression. *Mol Ther* **17**: 360–368.
11. Malecová, B and Morris, KV (2010). Transcriptional gene silencing through epigenetic changes mediated by non-coding RNAs. *Curr Opin Mol Ther* **12**: 214–222.
12. Suzuki, K and Kelleher, AD (2009). Transcriptional regulation by promoter targeted RNAs. *Curr Top Med Chem* **9**: 1079–1087.
13. Suzuki, K and Kelleher, AD. (2010). Lessons from viral latency in T cells: manipulating HIV-1 transcription by siRNA. *HIV Therapy* **4**: 199–213.
14. Ahlenstiel, CL, Lim, HG, Cooper, DA, Ishida, T, Kelleher, AD and Suzuki, K (2012). Direct evidence of nuclear Argonaute distribution during transcriptional silencing links the actin cytoskeleton to nuclear RNAi machinery in human cells. *Nucleic Acids Res* **40**: 1579–1595.
15. Knowling, S, Stapleton, K, Turner, AM, Uhlmann, E, Lehmann, T, Vollmer, J *et al.* (2012). Chemically Modified Oligonucleotides Modulate an Epigenetically Varied and Transient Form of Transcription Silencing of HIV-1 in Human Cells. *Mol Ther Nucleic Acids* **1**: e16.
16. Turner, AM, Ackley, AM, Matrone, MA and Morris, KV (2012). Characterization of an HIV-targeted transcriptional gene-silencing RNA in primary cells. *Hum Gene Ther* **23**: 473–483.
17. Turunen, MP, Lehtola, T, Heinonen, SE, Assefa, GS, Korpisalo, P, Girnary, R *et al.* (2009). Efficient regulation of VEGF expression by promoter-targeted lentiviral shRNAs based on epigenetic mechanism: a novel example of epigenetherapy. *Circ Res* **105**: 604–609.
18. Novina, CD, Murray, MF, Dykxhoorn, DM, Beresford, PJ, Riess, J, Lee, SK *et al.* (2002). siRNA-directed inhibition of HIV-1 infection. *Nat Med* **8**: 681–686.
19. Jacque, JM, Triques, K and Stevenson, M (2002). Modulation of HIV-1 replication by RNA interference. *Nature* **418**: 435–438.
20. Boden, D, Pusch, O, Lee, F, Tucker, L and Ramratnam, B (2003). Human immunodeficiency virus type 1 escape from RNA interference. *J Virol* **77**: 11531–11535.
21. Das, AT, Brummelkamp, TR, Westerhout, EM, Vink, M, Madiredjo, M, Bernards, R *et al.* (2004). Human immunodeficiency virus type 1 escapes from RNA interference-mediated inhibition. *J Virol* **78**: 2601–2605.
22. von Eije, KJ, ter Brake, O and Berkhout, B (2008). Human immunodeficiency virus type 1 escape is restricted when conserved genome sequences are targeted by RNA interference. *J Virol* **82**: 2895–2903.
23. Westerhout, EM, Ooms, M, Vink, M, Das, AT and Berkhout, B (2005). HIV-1 can escape from RNA interference by evolving an alternative structure in its RNA genome. *Nucleic Acids Res* **33**: 796–804.
24. Shah, PS, Pham, NP and Schaffer, DV (2012). HIV develops indirect cross-resistance to combinatorial RNAi targeting two distinct and spatially distant sites. *Mol Ther* **20**: 840–848.
25. ter Brake, O, Konstantinova, P, Ceylan, M and Berkhout, B (2006). Silencing of HIV-1 with RNA interference: a multiple shRNA approach. *Mol Ther* **14**: 883–892.
26. Wassenegger, M, Heimes, S, Riedel, L and Sänger, HL (1994). RNA-directed de novo methylation of genomic sequences in plants. *Cell* **76**: 567–576.
27. Wassenegger, M (2000). RNA-directed DNA methylation. *Plant Mol Biol* **43**: 203–220.
28. Mette, MF, Matzke, AJ and Matzke, MA (2001). Resistance of RNA-mediated TGS to HC-Pro, a viral suppressor of PTGS, suggests alternative pathways for dsRNA processing. *Curr Biol* **11**: 1119–1123.
29. Jones, L, Ratcliff, F and Baulcombe, DC (2001). RNA-directed transcriptional gene silencing in plants can be inherited independently of the RNA trigger and requires Met1 for maintenance. *Curr Biol* **11**: 747–757.
30. Sibley, CR, Seow, Y and Wood, MJ (2010). Novel RNA-based strategies for therapeutic gene silencing. *Mol Ther* **18**: 466–476.
31. Roberts, TC, Andaloussi, SE, Morris, KV, McClorey, G and Wood, MJ (2012). Small RNA-Mediated Epigenetic Myostatin Silencing. *Mol Ther Nucleic Acids* **1**: e23.
32. Miller, V and Larder, BA (2001). Mutational patterns in the HIV genome and cross-resistance following nucleoside and nucleotide analogue drug exposure. *Antivir Ther (Lond)* **6**(suppl. 3): 25–44.
33. Klenerman, P, Wu, Y and Phillips, R (2002). HIV: current opinion in escapology. *Curr Opin Microbiol* **5**: 408–413.
34. Suzuki, K, Juelich, T, Lim, H, Ishida, T, Watanebe, T, Cooper, DA *et al.* (2008). Closed chromatin architecture is induced by an RNA duplex targeting the HIV-1 promoter region. *J Biol Chem* **283**: 23353–23363.
35. Weinberg, MS, Barichievy, S, Schaffer, L, Han, J and Morris, KV (2007). An RNA targeted to the HIV-1 LTR promoter modulates indiscriminate off-target gene activation. *Nucleic Acids Res* **35**: 7303–7312.
36. Jackson, AL, Bartz, SR, Schelter, J, Kobayashi, SV, Burchard, J, Mao, M *et al.* (2003). Expression profiling reveals off-target gene regulation by RNAi. *Nat Biotechnol* **21**: 635–637.
37. Hornung, V, Guenthner-Biller, M, Bourquin, C, Ablasser, A, Schlee, M, Uematsu, S *et al.* (2005). Sequence-specific potent induction of IFN-alpha by short interfering RNA in plasmacytoid dendritic cells through TLR7. *Nat Med* **11**: 263–270.
38. Judge, AD, Sood, V, Shaw, JR, Fang, D, McClintock, K and MacLachlan, I (2005). Sequence-dependent stimulation of the mammalian innate immune response by synthetic siRNA. *Nat Biotechnol* **23**: 457–462.
39. Suzuki, K, Shijuuku, T, Fukamachi, T, Zaunders, J, Guillemin, G, Cooper, D *et al.* (2005). Prolonged transcriptional silencing and CpG methylation induced by siRNAs targeted to the HIV-1 promoter region. *J RNAi Gene Silencing* **1**: 66–78.
40. Lim, HG, Suzuki, K, Cooper, DA and Kelleher, AD (2008). Promoter-targeted siRNAs induce gene silencing of simian immunodeficiency virus (SIV) infection *in vitro*. *Mol Ther* **16**: 565–570.
41. Yamagishi, M, Ishida, T, Miyake, A, Cooper, DA, Kelleher, AD, Suzuki, K *et al.* (2009). Retroviral delivery of promoter-targeted shRNA induces long-term silencing of HIV-1 transcription. *Microbes Infect* **11**: 500–508.

42. Suzuki, K, Ishida, T, Yamagishi, M, Ahlenstiel, C, Swaminathan, S, Marks, K *et al.* (2011). Transcriptional gene silencing of HIV-1 through promoter targeted RNA is highly specific. *RNA Biol* **8**: 1035–1046.
43. Hattori, S, Ide, K, Nakata, H, Harada, H, Suzu, S, Ashida, N *et al.* (2009). Potent activity of a nucleoside reverse transcriptase inhibitor, 4'-ethynyl-2-fluoro-2'-deoxyadenosine, against human immunodeficiency virus type 1 infection in a model using human peripheral blood mononuclear cell-transplanted NOD/SCID Janus kinase 3 knockout mice. *Antimicrob Agents Chemother* **53**: 3887–3893.
44. Weinberg, MS, Villeneuve, LM, Ehsani, A, Amarzguioui, M, Aagaard, L, Chen, ZX *et al.* (2006). The antisense strand of small interfering RNAs directs histone methylation and transcriptional gene silencing in human cells. *RNA* **12**: 256–262.
45. Brummelkamp, TR, Bernards, R and Agami, R (2002). A system for stable expression of short interfering RNAs in mammalian cells. *Science* **296**: 550–553.
46. Colin, L and Van Lint, C (2009). Molecular control of HIV-1 postintegration latency: implications for the development of new therapeutic strategies. *Retrovirology* **6**: 111.
47. Folks, TM, Justement, J, Kinter, A, Dinarello, CA and Fauci, AS (1987). Cytokine-induced expression of HIV-1 in a chronically infected promonocyte cell line. *Science* **238**: 800–802.
48. Della Chiara, G, Crotti, A, Liboi, E, Giacca, M, Poli, G and Lusic, M (2011). Negative regulation of HIV-1 transcription by a heterodimeric NF-κB1/p50 and C-terminally truncated STAT5 complex. *J Mol Biol* **410**: 933–943.
49. Matalon, S, Rasmussen, TA and Dinarello, CA (2011). Histone deacetylase inhibitors for purging HIV-1 from the latent reservoir. *Mol Med* **17**: 466–472.
50. Zhou, J, Neff, CP, Liu, X, Zhang, J, Li, H, Smith, DD *et al.* (2011). Systemic administration of combinatorial dsiRNAs via nanoparticles efficiently suppresses HIV-1 infection in humanized mice. *Mol Ther* **19**: 2228–2238.
51. Neff, CP, Zhou, J, Remling, L, Kuruvilla, J, Zhang, J, Li, H *et al.* (2011). An aptamer-siRNA chimera suppresses HIV-1 viral loads and protects from helper CD4(+) T cell decline in humanized mice. *Sci Transl Med* **3**: 66ra6.
52. ter Brake, O, Legrand, N, von Eije, KJ, Centlivre, M, Spits, H, Weijer, K *et al.* (2009). Evaluation of safety and efficacy of RNAi against HIV-1 in the human immune system (Rag-2(-/-)gammac(-/-)) mouse model. *Gene Ther* **16**: 148–153.
53. Shimizu, S, Hong, P, Arumugam, B, Pokomo, L, Boyer, J, Koizumi, N *et al.* (2010). A highly efficient short hairpin RNA potently down-regulates CCR5 expression in systemic lymphoid organs in the hu-BLT mouse model. *Blood* **115**: 1534–1544.
54. Centlivre, M, Legrand, N, Klamer, S, Liu, YP, Eije, KJ, Bohne, M *et al.* (2013). Preclinical *In Vivo* Evaluation of the Safety of a Multi-shRNA-based Gene Therapy Against HIV-1. *Mol Ther Nucleic Acids* **2**: e120.
55. Freed, EO and Martin MA (2001). HIVs and their replication. *Fields Virology*. Lippincott Williams & Wilkins: New York.
56. Jeang, KT, Xiao, H and Rich, EA (1999). Multifaceted activities of the HIV-1 transactivator of transcription, Tat. *J Biol Chem* **274**: 28837–28840.
57. Greene, WC and Peterlin, BM (2002). Charting HIV's remarkable voyage through the cell: basic science as a passport to future therapy. *Nat Med* **8**: 673–680.
58. Kalebic, T, Kinter, A, Poli, G, Anderson, ME, Meister, A and Fauci, AS (1991). Suppression of human immunodeficiency virus expression in chronically infected monocytic cells by glutathione, glutathione ester, and N-acetylcysteine. *Proc Natl Acad Sci USA* **88**: 986–990.
59. Okada, S, Harada, H, Ito, T, Saito, T and Suzu, S (2008). Early development of human hematopoietic and acquired immune systems in new born NOD/Scid/Jak3null mice intrahepatic engrafted with cord blood-derived CD34 + cells. *Int J Hematol* **88**: 476–482.
60. Fernandez, G and Zeichner, SL (2010). Cell line-dependent variability in HIV activation employing DNMT inhibitors. *Virol J* **7**: 266.
61. Wightman, F, Ellenberg, P, Churchill, M and Lewin, SR (2012). HDAC inhibitors in HIV. *Immunol Cell Biol* **90**: 47–54.
62. Miyoshi, H, Takahashi, M, Gage, FH and Verma, IM (1997). Stable and efficient gene transfer into the retina using an HIV-based lentiviral vector. *Proc Natl Acad Sci USA* **94**: 10319–10323.
63. Zhang, B, Xia, HQ, Cleghorn, G, Gobe, G, West, M and Wei, MQ (2001). A highly efficient and consistent method for harvesting large volumes of high-titre lentiviral vectors. *Gene Ther* **8**: 1745–1751.
64. Suzuki, K, Craddock, BP, Okamoto, N, Kano, T and Steigbigel, RT (1993). Poly A-linked colorimetric microtiter plate assay for HIV reverse transcriptase. *J Virol Methods* **44**: 189–198.

Supplementary Information accompanies this paper on the Molecular Therapy–Nucleic Acids website (http://www.nature.com/mtna)

Cancer Science
The official journal of the Japanese Cancer Association

Human T-cell leukemia virus type 1 Tax protein interacts with and mislocalizes the PDZ domain protein MAGI-1

Grace Naswa Makokha,[1] Masahiko Takahashi,[1] Masaya Higuchi,[1] Suguru Saito,[1] Yuetsu Tanaka[2] and Masahiro Fujii[1,3]

[1]Division of Virology, Niigata University Graduate School of Medical and Dental Sciences, Niigata; [2]Department of Immunology, Graduate School and Faculty of Medicine, University of the Ryukyus, Okinawa, Japan

(Received July 5, 2012/Revised November 18, 2012/Accepted December 14, 2012/Accepted manuscript online December 20, 2012/Article first published online January 30, 2013)

Human T-cell leukemia virus type 1 (HTLV-1) is the etiological agent of adult T-cell leukemia (ATL). HTLV-1 encodes the oncoprotein Tax1, which is essential for immortalization of human T-cells and persistent HTLV-1 infection *in vivo*. Tax1 has a PDZ binding motif (PBM) at its C-terminus. This motif is crucial for the transforming activity of Tax1 to a T-cell line and persistent HTLV-1 infection. Tax1 through the PBM interacts with PDZ domain proteins such as Dlg1 and Scribble, but it has not been determined yet, which cellular PDZ proteins mediate the functions of Tax1 PBM. Here we demonstrate that Tax1 interacts with the PDZ domain protein MAGI-1 in a PBM-dependent manner, and the interaction mislocalizes MAGI-1 from the detergent-soluble to the detergent-insoluble cellular fraction in 293T cells and in HTLV-1-infected T-cells. In addition, Tax1-transformation of a T-cell line from interleukin (IL)-2-dependent to IL-2-independent growth selects cells with irreversibly reduced expression of MAGI-1 at mRNA level. These findings imply that Tax1, like other viral oncoproteins, targets MAGI-1 as a mechanism to suppress its anti-tumor functions in HTLV-1-infected cells to contribute to the transforming activity of T-cells and persistent HTLV-1 infection. (*Cancer Sci* 2013; 104: 313–320)

Human T-cell leukemia virus type 1 (HTLV-1) is the etiological agent of adult T-cell leukemia (ATL).[1,2] Among several non-structural genes encoded by HTLV-1, Tax1 is a crucial regulator of viral life cycle as a potent transcriptional activator for its own transcription.[3–5] In addition, Tax1 is a key player involved in T-cell immortalization, transformation, persistent infection, inflammation, and leukemogenesis.[6–11] All these pleitropic functions of Tax1 are believed to be directed by a wide spectrum of interactions with cellular factors. For instance, numerous PDZ domain containing cellular proteins have been shown to complex with Tax1 through the PDZ binding motif (PBM) located at its C-terminus.[12,13] We have previously shown that the PBM plays a key role in Tax1 mediated activities. The motif was critically involved in Tax1-induced transformation of a rat fibroblast cell line and a mouse T-cell line.[14,15] Moreover, an HTLV-1ΔPBM virus with a deletion of the Tax1 PBM in HTLV-1, failed to establish persistent infection in rabbits as measured by lack of antibody response against HTLV-1 and the absence of HTLV-1 proviruses.[16]

Human T-cell leukemia virus type 2 (HTLV-2) is closely related to HTLV-1, but it is unable to cause any malignancy.[17,18] One notable difference between the two is the lack of PBM in Tax2, and thus Tax1 PBM is proposed to be one of the major determinants of HTLV-1 pathogenesis.[14,19] Intriguingly, PBMs have been identified in other viral oncoproteins such as the E4-ORF1 protein of human adenovirus type 9 and the E6 proteins of high-risk human papilloma viruses (HPV),[20–22] suggesting that the oncogenic ability of these viruses may depend in part on interactions involving their PBMs with cellular proteins.

PSD-95/Disc Large/Zona Occludens-1 (PDZ) domain containing proteins form signaling complexes at the inner surface of cell membrane and are involved in a broad range of functions like cell signaling, cell–cell adhesion, tight junction integrity, molecular scaffolding for protein complexes, and tumor suppression.[23,24] The human genome contains hundreds of PDZ domain containing proteins,[25] and some of them have been shown to be targeted by viral oncoproteins.[26–29] Tax1 selectively interacts with Dlg1 and Scribble.[13,30] Of the two, Dlg1 has been widely studied due to its involvement in cell growth signaling and tumor suppression.[31–33] Our previous findings suggested that inactivation of Dlg1 increases the ability of Tax1 to transform a mouse T-cell line (CTLL-2) from interleukin (IL)-2-dependent to IL-2-independent growth, but it did not increase such transforming activity in a PBM defective Tax1 mutant.[34] Hence we concluded that other yet unidentified PDZ protein(s) besides Dlg1 likely inhibit(s) transformation of CTLL-2 by Tax1 and inactivation of these proteins by Tax1 is essential for the transformation of CTLL-2.

MAGI-1 (MAGUK with inverted domain structure 1) is a PDZ protein closely related to Dlg1,[35] and it has also been implicated in tumor suppression in various systems. For instance, MAGI-1 suppressed invasion of tumor cells by recruiting PTEN/β-catenin complex to the adherent junctions and downregulation of phosphatidylinositol 3-kinases (PI3K) signaling.[36] MAGI-1 is a known target of viral oncoproteins adenovirus-9 E4-ORF1 and high-risk HPV E6.[37,38] In the present research, we provide evidence that MAGI-1 is targeted by the HTLV-1 oncoprotein Tax1 in two independent mechanisms. Tax1 interacts with MAGI-1 and alters the subcellular localization. In addition, a low MAGI-1 expression is selected during Tax1-immortalization of human T-cells and IL-2-independent transformation of CTLL-2 cells. Interestingly, unlike Tax1, Tax2-immortalization of human T-cells is not associated with downregulation of MAGI-1 expression. These findings suggest that MAGI-1, a PDZ protein known to be associated with tumour suppression, is an important cellular target of HTLV-1 Tax1 for T-cell immortalization and transformation.

Materials and Methods

Cell lines and cell culture. The human embryonic kidney cell line 293T was cultured in DMEM supplemented with 10% FBS, 50 U/mL penicillin, and 50 μg/mL streptomycin. The human T-cell lines used in the present experiments have been

[3]To whom correspondence should be addressed.
E-mail: fujiimas@med.niigata-u.ac.jp

doi: 10.1111/cas.12087

characterized previously.[14] PBL/HTLV-1 and PBL/HTLV-1ΔPBM are IL-2-dependent HTLV-1-immortalized human T-cell lines, and they were established as previously described.[16] SLB-1, MT-4 and HUT-102 are IL-2-independent HTLV-1-transformed human T-cell lines. HUT78, MOLT-4 and Jurkat are HTLV-1-negative human T-cell lines. SLB-1, HUT-102, HUT78, MT-4, MOLT-4 and Jurkat cells were cultured in RPMI 1640 supplemented with 10% FBS, 4 mM glutamine, penicillin (50 U/mL), and streptomycin (50 μg/mL) (RPMI/10%FBS). PBL/HTLV-1 and PBL/HTLV-1ΔPBM were cultured in RPMI/20%FBS with 1 nM recombinant human IL-2 (Takeda Chemical Industries, Osaka, Japan). CTLL-2 is a mouse cytotoxic T-cell line that grows in an IL-2-dependent manner,[6,15] and was cultured in RPMI/10%FBS containing 2-mercaptoethanol (2-ME) and 1 nM IL-2. CTLL-2 cells stably expressing hAkt1ΔmPH were described previously.[39] They were cultured in RPMI/10%FBS containing 2-ME, 1 nM IL-2 and 0.5 mg/mL G418 (Invitrogen, Carlsbad, CA, USA). Tax1- and hAkt1ΔmPH-transformed IL-2-independent CTLL-2 cells were established as described previously,[34,39] and cultured in RPMI/10%FBS containing 2-ME but without IL-2.

Plasmids. The expression plasmids pHβPr-neo-Tax1 and pHβPr-neo-Tax1ΔC that were used for the expression of Tax1 and Tax1ΔC respectively in 293T cells together with the lentiviral vector CSII-EF-IG-RfA used for the generation of recombinant lentiviruses for expression of Tax1 in T-cells have been described previously.[40,41] Tax1ΔC is a PBM-negative mutant, with a four amino acid deletion from the C-terminus of Tax1.[14] pcDNA3.1:FLAG-MAGI-1c (A gift from L. Banks, International Centre for Genetic Engineering and Biotechnology, Italy), was constructed by cloning FLAG-MAGI-1c into the HindIII/EcoRI site of pcDNA3.1 (Invitrogen) with a FLAG-tag at the N-terminus.

Western blotting analysis. Cells were lysed with the SDS-sample buffer consisting of 62.5 mM Tris-HCl (pH 6.8), 2% SDS, 10% glycerol. Protein concentrations of the cell lysates were measured using the DC protein assay kit (Bio-Rad Laboratories, Hercules, CA, USA). The cell lysates (20 μg) were then treated with 50 mM DTT, 0.01% bromophenol blue, and heated at 95°C for 5 min. The resultant lysates were subjected to SDS-PAGE separation. The proteins in the gel were transferred to a nitrocellulose membrane, which was then incubated with 5% skim milk for 1 h at room temperature to inhibit non-specific binding, and further incubated with the primary antibody. After washing with TNN buffer (10 mM Tris–HCl [pH 7.5], 50 mM NaCl, and 0.05% NP40), the membranes were further incubated with either anti-mouse or anti-rabbit immunoglobulins conjugated with horseradish peroxidase (Bio-Rad Technologies) as secondary antibodies. Proteins recognized by the antibodies in the membrane were visualized using the ECL Western blotting detection system (Amersham Biosciences, Piscataway, NJ, USA). Primary antibodies used above were mouse anti-Tax1 mAb (TAXY-7),[42] rabbit anti-Tax2 pAb,[43] mouse anti-FLAG M2 mAb, rabbit anti-MAGI-1 antibody (Sigma-Aldrich, Tokyo, Japan), rabbit anti-Akt mAb (Cell Signaling Technology, Beverly, MA, USA), mouse anti-Syntrophin-β mAb (Affinity Bioreagents, Golden, CO, USA) and mouse anti-α-Tubulin mAb (Oncogene Research Products, San Diego, CA, USA). The above named anti-Tax1 and anti-MAGI-1 antibodies were also used for the immunoprecipitation and immunoflorescence assays.

Immunoflorescence. To analyze the subcellular localization of Tax1 and MAGI-1 in 293T cells, the cells were cultured on glass slides in a six-well culture plate overnight, and transiently transfected with pHβPr-neo, pHβPr-neo-Tax1, or pHβPr-neo-Tax1ΔC plasmid using the lipofection method (FUGENE 6; Roche Diagnostics, Tokyo, Japan). At 48 h after transfection, the cells were fixed with 4% formaldehyde in PBS for 25 min at 4°C and permeabilized by 0.1% TritonX-100. The fixed cells were then incubated with the rabbit anti-MAGI-1 antibody and the mouse anti-Tax1 antibody for 30 min. After washing the slides with PBS, the cells were incubated with Alexa594-labeled anti-mouse IgG, Alexa488-labeled anti-rabbit IgG (Molecular Probes) alongside Hoechst 33258 for another 30 min. The stained cells were then examined by fluorescent microscopy (BZ-8000; KEYENCE, Osaka, Japan) for analysis.

Co-immunoprecipitation. The Tax1 plasmids were transiently transfected into 293T cells with or without the pcDNA3.1:FLAG-MAGI-1c (4 μg) by the lipofection method (FUGENE 6). At 48 h after the transfection, the cells were treated with the lysis buffer A (25 mM Tris [pH 7.2], 150 mM NaCl, 1.0 mM EDTA, 1% NP40, 2.0 mM phenylmethanesulfonyl fluoride, 20 μg/mL aprotinin, 1.0 mM Na_3VO_4, 1.0 mM NaF), after centrifugation of the cell lysates, the supernatants were immunoprecipitated with anti-Tax1 antibody. The amount of Tax1 and MAGI-1 proteins in the precipitates was analyzed by a Western blotting analysis using anti-Tax1, and anti-MAGI-1 or anti-FLAG M2 antibodies, respectively.

Cell fractionation. The 293T cells were transfected with Tax1 and its mutant plasmid by the lipofection method (FUGENE 6). At 48 h after transfection, the cells were divided into two groups. One was treated with the lysis buffer A (described above) at 4°C for 15 min. After centrifugation, the supernatant was collected and used as the soluble fraction, and the resultant pellet was further treated with the SDS-sample buffer (125 mM Tris–HCl [pH 6.8], 2% SDS, 20% glycerol, 0.01% bromophenol blue, and 10% β-mercaptoethanol) at 4°C for 15 min. The lysates were used as the insoluble fraction. The other group was directly treated with the SDS-sample buffer and used as the total fraction. A similar cell fractionation assay was performed for HTLV-1-negative (Jurkat) and HTLV-1-positive (SLB-1) T-cells. The three sets of samples were separately size-fractionated by SDS-PAGE, and the amounts of proteins were measured by a Western blotting analysis.

Immortalization of PBMCs. Human peripheral blood mononuclear cells (PBMCs) were isolated from the blood of healthy donors. They were stimulated with 10 μg/mL phytohemagglutinin (PHA) (Sigma Aldrich) in RPMI/20%FBS supplemented with 55 μM 2-ME for 2 days, and then further cultured in RPMI/20%FBS with 0.5 nM IL-2 and 2-ME for 2 days. A portion of these cells was set aside to be used as Tax untreated PBMCs. Immortalization of PBMCs by Tax1 and Tax2 was carried out as we recently described.[44]

Transient transfection assays. To generate recombinant lentiviruses, 293T cells were transfected with pCAG-HIVgp, pCMV-VSV-G-RSV-Rev (provided by Dr H. Miyoshi) and the respective lentiviral vectors encoding Tax1 or Tax1ΔC using FUGENE 6. At 72 h after the transfection, the supernatant was collected and used to infect CTLL-2 and Jurkat cells at 4×10^5 cells/well in a 12-well plate in a final volume of 2 mL medium. At 48 h after transfection, cell lysates were prepared from the transfected cells and used for a Western blotting analysis.

RNA extraction and quantitative real-time RT-PCR. All reagents used were acquired from TAKARA BIO Japan. The assay was carried out according to the manufacturer's instructions. Total RNA was extracted by the Fast Pure RNA kit and 1 μg was used for cDNA synthesis using the Prime Script RT reagent kit. Two-step 40-cycle quantitative real-time RT-PCR for MAGI-1 expression was carried out by the Thermal Cycler Dice Real Time system and the DNA master SYBR Green using the primers 5′-GCACTGGATGGCAAGATGGA-3′ and 5′-ACCAATGGGAATGGACTGGAAG-3′ for both mouse and human MAGI-1. Amplification of each template was

doi: 10.1111/cas.12087